The microtubule protein Doublecortin contributes to maintenance of bipolar shape and nuclear translocation during neuronal migration in the adult forebrain

Hiroyuki Koizumi, Holden Higginbotham, Tiffany Poon, Teruyuki Tanaka, Brendan C. Brinkman, Joseph G. Gleeson*

Neurogenetics Laboratory
Department of Neurosciences
University of California, San Diego

*To whom correspondence should be addressed.
Joseph G. Gleeson
jogleeson@ucsd.edu
Leichtag 3A16
9500 Gilman Dr.
La Jolla, CA 92093-0691
Ph: 858-822-3535
Fax: 858-822-1021

ABSTRACT

The ability of the mature mammalian nervous system to continually produce neuronal precursors is of considerable importance, as manipulation of this process might one day permit the replacement of cells lost as a result of injury or disease. In mammals, the anterior subventricular zone (SVZa) region is one of the primary sites of adult neurogenesis. Here we show that Doublecortin (DCX), a widely used marker for newly generated neurons, when deleted in mouse results in a severe morphological defect in the rostral migratory stream and delayed neuronal migration that is independent of direction or responsiveness to Slit chemorepulsion. DCX is required for nuclear translocation and maintenance of bipolar morphology during migration of these cells. Our data identifies a critical function for DCX in the movement of newly generated neurons in the adult brain.

In the rodent and primate brain, the anterior region of the lateral ventricle and the hippocampus are the primary sites of adult neurogenesis [1-7]. These neuroblasts, upon completing migration, are capable of maturing into fully differentiated neurons, integrating into local synaptic circuits and may be important in adult cognitive processing [8-11].

The mechanisms controlling the targeted translocation of large numbers of cells to the olfactory bulb (OB) over a considerable distance (>5 mm in the adult mouse) are an issue of intense investigation. These neurons translocate using a process known as chain migration, whereby the cells use each other as the migratory substrate [12]. These newly generated neurons are derived from SVZa glial fibrillary acidic protein (GFAP)-positive astrocytes [13, 14], which also ensheath them as they move through extensive interconnected networks along the lining of the lateral ventricle in the rostral forebrain and the rostral migratory stream (RMS) [15]. There, they are under the control of extracellular migration guidance cues, including the secreted ligands Slit and Reelin [16-19], the receptors ErbB4 and Deleted in Colorectal Carcinoma (DCC) [20, 21], as well as integrins and neural cell adhesion molecule [21-23]. Upon reaching the bulb, the neurons turn and migrate in a radial direction [24], integrating into either the granule cell layer or the periglomerular network [25].

The X-linked gene *doublecortin* (*DCX*) is mutated in some patients with the severe neuronal migration defect called classical lissencephaly or double cortex syndrome [26, 27]. This migration defect is likely to be cell autonomous, because in females with a heterozygous mutation, approximately half of the neurons are misplaced within the cerebral cortex as would be expected from random X-chromosome inactivation. As a result, males display a four-layered agyric cortex and females display a subcortical band of heterotopic neurons. It was surprising, therefore, that the *Dcx* knockout mice displayed no appreciable defect in cortical neuronal lamination or positioning [28]. One possible explanation for these species differences is the order-of-magnitude greater distance (approximately 2-3 cm vs. 2-3 mm) and greater time window (10 wks vs. 7 d) for cortical neuronal migration in humans vs. rodent, respectively [29]. We therefore tested for disrupted neuronal migration in adult *Dcx* knockout mouse SVZa, where neurons migrate greater distances (up to 5 mm) throughout the life of the animal.

RESULTS

DCX expression in the RMS

We determined that DCX is expressed at high levels in a population of cells within the SVZa, along the RMS and remains detectable in these cells as they migrate into the OB [30-32] (Supplemental Fig. 1). DCX expression is downregulated in postmigratory neurons within the granule cell layer and glomerular layer of the OB (not shown). The only other location of appreciable DCX expression in adult brain was in a small number of hippocampal subgranular layer cells (not shown). The polysialylated form of neural cell adhesion molecule (PSA-NCAM) as well as β3-tubulin (TuJ1) mark early committed neurons that are located within the RMS [33, 34]. We found co-distribution of DCX with PSA-NCAM and TuJ1 in these regions. The expression pattern of DCX appeared to be more specific than PSA-NCAM for neurons within the RMS, with less background staining in other anatomic regions (Supplemental Fig. 1b, c). There was near complete concordance of DCX expression compared with either marker within the RMS (Supplemental Fig. 1d, e). After careful examination, we could not identify any cells within the RMS that were not double-stained using this approach. We conclude that

DCX is selectively expressed by migratory populations of cells within the SVZa, RMS and proximal OB.

Deletion of *Dcx* results in morphological defects of the RMS

Because *Dcx -/y* males do not mate well, we focused our analysis on male *Dcx -/y* and *Dcx +/y* littermates, which result in equal numbers from intercross of *Dcx +/y* males and *Dcx +/-* females. Parasagittal sections from adult mice (P49-56) through the SVZa, RMS and OB were stained using Cresyl violet to delineate the cell-dense RMS [22]. Surprisingly, we found a significant alteration in the morphology of the SVZa and RMS, with these structures approximately doubled in thickness along much of their length. This increased thickness was noted along the length of the RMS through the rostral flexure in the region of the septum, where it appeared to revert to a normal thickness (Fig. 1a, b). Approximately 10 mice from each genotype were analyzed using this method, and all *Dcx -/y* displayed a similar appearance. In order to be certain that this morphological defect was not dependent on the lateral-medial plane of sampling, we sectioned in the coronal plane and again observed an increased width of the RMS along its entire length (Fig. 1c, d). We also compared serial sections, and found an increased size of the RMS along its length as expected (Supplemental Fig. 2). We conclude that the RMS is enlarged in the absence of *Dcx*.

To determine if this phenotype was present in female mutants, we additionally analyzed both *Dcx +/-* and *-/-* mice. By comparing aged-matched controls, we found that none of the four *Dcx +/-* mice examined had a thickened RMS (Supplemental Fig. 3a-f). As expected, however, the *Dcx -/-* female mice had a phenotype that was indistinguishable from *Dcx -/y* males, as both are complete null for *Dcx* in all cells (Supplemental Fig. 3g, i). We conclude that the RMS phenotype is fully expressive in both the complete null male and female mice.

We next performed the immunohistochemical study to determine if the increased size of RMS in mutant mice was due to an increase in the number of neurons, glia, or other cell types. Parasagittal sections through the RMS from *Dcx +/y* and *-/y* mice were stained with GFAP to label glia and either PSA-NCAM or TuJ1 to label early committed neurons. We noted that the increase in size of the RMS corresponded to an increase in

the width of the GFAP and PSA-NCAM cell stream (Fig. 1e, f). To determine if there was a defect in the ratio of neurons to glia, we estimated cell numbers by measuring total pixel number of GFAP vs. PSA-NCAM signal, and found no differences (data not shown), suggesting there is no alteration in the proportion of cell types in the expanded RMS. We noted the same close approximation of the GFAP and PSA-NCAM- or TuJ1-positive cells in both *Dcx +/y* and *-/y* brains. Three-dimensional reconstruction of confocal imaging *z*-stacks showed glial tubes encompassing chains of neuronal cells in both genotypes (not shown). In *Dcx +/y*, the orientation of glia and neurons was uniformly in the direction of migration, with glial and neuronal processes extending in the ventral and rostral direction (Fig. 1g, arrow), but in *Dcx -/y,* this was not always evident, and the orientation of glial and neuronal processes appeared not as well ordered as in wild-type (*wt*) (Fig. 1h, arrowheads).

We reasoned that these stalled migratory cells may take on one of several fates, so we tested for alterations in NeuN-positive cells (a marker for differentiated neurons) and activated caspase-3-positive neurons (CAS3, a marker for programmed cell death). The RMS in *Dcx -/y* mice contained many more NeuN-positive as well as CAS3-positive cells along its entire length compared with *wt* (Fig. 1i-l), suggesting that these cells that fail to migrate may differentiate to postmigratory neurons by default and /or died.

Newly generated neurons fail to migrate properly in *Dcx* knockout mice

The previous data suggested a delay or block in the ability of newly generated neurons to migrate into the OB, which was tested with BrdU birthdate labeling. First, we performed BrdU injections at P28, and then sacrificed animals 7 days later. In both *Dcx -/y* and *Dcx +/y* mice, approximately the same numbers of labeled neurons were present in the SVZa (Fig. 2a, b), suggesting that mitotic generation of neuroblasts is not affected by loss of *Dcx*. Analysis of the RMS, though, revealed a striking paucity of BrdU-positive neurons in more rostral regions (Fig. 2c, d). In *Dcx +/y* littermates, BrdU labeled a thin stream of neurons within the descending and rostral branch of the RMS, with the majority of labeled cells within the fanned-out region of the RMS and in the granule cell layer of the OB, suggesting that many of these neurons had migrated into this structure. In matched sections through the RMS in *Dcx -/y* mice, the majority of labeled cells were present

within the descending branch of the RMS in a thick collection that was reminiscent of PSA-NCAM/TuJ1/GFAP staining in mutants (see Fig. 1). There were very few labeled cells within the fanned-out region of the RMS and very few within the limits of the OB. Analysis of serial sections revealed an apparent variability in quantity of labeled neurons from a single mouse, but overall there were far fewer labeled neurons within the OB in the *Dcx* -/y mice compared with littermate *wt* controls, and none of the control mice displayed the massive collection of labeled neurons within the RMS. We conclude that DCX is required for migration of neurons within the RMS into the OB.

Many of these adult-born neurons eventually position within the glomerular layer of the OB and differentiate into GABAergic periglomerular interneurons, express unique marker subsets, [35] and survive for an extended period of time (over a year) [25]. In order to determine if migration of newly generated neurons to the final position in the OB is disrupted in *Dcx* knockout mice, we repeated the BrdU injections at P28, and then sacrificed animals 4 weeks later. We counted BrdU positive cells in the GL, and found only about half the number in *Dcx -/y* mice (Fig. 2e-g). In order to determine if specific populations of neurons are depleted in the absence of *Dcx*, sections from both mutant and *wt* mice were thus stained for calbindin (CB), calretinin (CR), parvalbumin (PV) and tyrosine hydroxylase (TH), some of the most widely used markers for these populations which stain largely distinct neuronal classes [35, 36]. In order to prevent sampling error due to the normal variability in the size of glomeruli and numbers of periglomerlular surrounding neurons, we sampled glomeruli from each of three OB regions (superior, rostral, inferior), obtained thick (50 μm) sections through the entire bulb, and counted the number of labeled neurons per glomerulus (for CB and CR) or neurons per standard area (for PV and TH). When compared with *wt* controls, *Dcx -/y* mice had significantly fewer CB-positive neurons (Fig. 2h-j), and somewhat reduced but not statistically significant differences in CR, PV and TH (Supplemental Fig. 4). There were no statistical differences in numbers of BrdU or marker positive cells in the external plexiform layer (EPL) or granule cell layer (GC), possibly due to the shorter distances that these neurons migrate (not shown). We conclude that defective migration leads to a reduction in the number of specific subsets of interneurons within the olfactory bulb.

Novel method for measuring migration within the RMS

The *in vivo* data suggested possible slowed or otherwise impaired migration. In order to test this, we utilized an RMS slice culture system to collect time-lapse images of labeled neurons from postnatal *Dcx +/y* and *-/y* littermates. We labeled the RMS with a crystal of DiI in P5 slices, and performed timelapse imaging of labeled migrating neurons. In *+/y* slices, we found many migrating DiI-positive neurons during a 1-2 hour recording, whereas in *-/y* slices, very few of the neurons showed similar movements (Fig. 3a). However, the number of labeled cells that could be identified in each microscopic field was low, and there was significant inter-experiment variability in migration speeds. These negative factors may have been a result of phototoxicity or damage to the RMS induced by manipulating the DiI crystal. An alternative method is transgenic labeling of cells with a fluorescent reporter. We tested transgenic mice that expressed GFP under the control of the *Dcx* promoter (*Dcx::EGFP* [37] and unpublished), because this model should allow visualization of the whole population of migrating RMS neurons. Strong GFP signal was exclusively found in the SVZ, RMS and OB in both adult (not shown) and P5 (Fig. 3b), which overlapped precisely with DCX expression. We utilized multiphoton microscopy, which minimizes photobleaching and phototoxicity and has intrinsic *z*-axis resolution [38]. Using this system, recordings of neuronal migration were captured for as long as 24 hours in P5 slices without an apparent decrease in migration rate or viability of the slice. This transgenic line was next crossed with *Dcx +/-*, to generate *Dcx -/y; Dcx::EGFP* mice. Acute brain sections through the RMS showed no alteration in GFP intensity within individual cells in *wt* and mutant sections. We conclude that this model can provide for long-term visualization of migrating neurons.

Defect in average velocity reflects "stutter" in migration initiation

In the *Dcx -/y; Dcx::EGFP* mice, as expected, we noted a significant increase in the number of GFP-positive cells within the RMS (see Fig. 1i, j). Comparison of movies from five separate experiments from each genotype showed overall slowed migration in *Dcx -/y* slices. In these experiments, neurons in *wt* slices typically displayed bipolar or monopolar morphology and migrated at saltatory rates throughout the recording, whereas in mutant slices neurons displayed frequent multipolar morphology that tended to

correlate with a long pause in migration. The multipolar phenotype and delayed migration rates appeared the same as in DiI-labeled migrating neurons. Assessment of merged datasets (by tracking the position of individual neurons in the *x-y-t* dimension) showed that some mutant neurons were capable of rapid migration for brief periods, but this was frequently interrupted by long stuttering-like pauses where cell bodies oscillated slightly (Fig. 3c and Supplemental Movie 1-2). We found that average velocity was decreased from 0.54 to 0.22 μm/min in mutant slices (Fig. 3d). Because movement of neurons is stochastic and may not follow a normal distribution, we also ranked the average velocity per neuron. We noted that mutant neurons were capable of migrating at speeds approaching *wt* neurons, but displayed rates that were, on average, significantly slower (Fig. 3e). Notably, there was no significant difference in the direction of migration or the maximum velocity achieved by each neuron during the recording (Fig. 3f, g). We conclude that average velocity is primarily affected in the *Dcx* -/y, which is likely a reflection of an increase in migration "stutter", as evidenced by long migration pauses.

Decreased migration of neurons exiting SVZa but no apparent defect in Slit responsiveness

These migration defects suggest a cell-intrinsic block in the ability of SVZa-derived neurons to migrate properly. In order to test this, we monitored migration of neurons exiting P5 *Dcx +/y* and *-/y* SVZa explants *in vitro*. In the *wt*, there was robust migration away from the explant over the 12-hour timecourse of the experiment [17, 39]. Parallel experiments performed with mutant explants showed a severe reduction in neuronal migration, without an apparent effect on cell exit from the explant (Fig. 4a). Approximately the same number of neurons extended neurites away from the explant and appeared to have initiated migration in both genotypes, but mutant cells failed to achieve similar migration distances from the edge of the reaggregates. Quantification of this effect from three separate experiments showed a significant reduction in the mean migration distance from the edge of the explant by over 50% (Fig. 4b). Separate experiments using timelapse analysis of migration velocity from over 100 neurons from

each genotype also showed a significant reduction (Fig. 4c). We conclude that DCX is required for migration of SVZa-derived neurons *in vitro*.

We considered that the migration defect might be the result of an inability to transduce extracellular guidance cues such as Slit to the neuronal cytoskeleton, as this is a major extracellular guidance cue of SVZa migration [17] and evidence suggests specific cytoskeletal proteins may transduce extracellular guidance cues [40, 41]. Slit application to explants results in the vast majority of neurons reversing polarization within 2 hours, and subsequently migrating back into the explant over the next 2-4 hours (Supplemental Fig. 5a depicts schematic). During neuronal repolarization, there is withdrawal of the previous leading process and extension of a new process in the new direction of migration that is dependent on an intact neuronal cytoskeleton (not shown). In response to Slit, approximately 70-75% of cells from both *Dcx +/y* and *-/y* explants underwent repolarization (Supplemental Fig. 5b, c), and there was no statistical difference between the datasets (Supplemental Fig. 5d). We conclude that *Dcx -/y* neurons do not display a defect in response to Slit stimulation.

Defect in *Dcx* null neurons in nuclear translocation events per peak in nuclear-centrosome distance.

Neuronal migration consists of a repeating of three basic events: 1. Leading process extension. 2. Positioning of the centrosome in the leading process. 3. Translocation of the nucleus towards the position of the centrosome [42]. As DCX localizes to the microtubules of the perinuclear cage, the leading process and the growth cones [43-45], we examined for defects in each of these. We first tested for a defect in the latter two events. The N-C distance (distance between the centrosome and the leading edge of the nucleus) is thought to reflect a dynamic interplay between movement of these two organelles, and altered N-C distance has been proposed to underlie the migration defect in some cell models [45-48]. A decrease in N-C distance should reflect a defect in centrosome positioning (event 2), whereas an increase should reflect a defect in nuclear translocation (event 3). We therefore measured N-C distance by first mating *Dcx +/-* with *β–actin::Cetn2-EGFP* mice, which expresses a Centrin2-GFP fusion protein under the control of the chick *β*–actin promoter [49]. Previous data has indicated that neurons from this transgenic mouse

display a single pair of fluorescent centrioles and intact centrosome behavior. SVZa explants from the resultant *Dcx -/y; β–actin::Cetn2-EGFP* and *Dcx* +/y; *β–actin::Cetn2-EGFP* littermates were similarly cultured and subject to time-lapse fluorescent imaging to visualize the nuclear outline and the centrosome. We detected no significant difference in average N-C distance between wt and mutant neurons (Fig. 4d). However, it was clear that the mutant cells display a defect in nucleokinesis, as the nuclei failed to translocate at the proper rate (see Fig. 4c). To test for a specific defect in the coupling of centrosome positioning to nucleokinesis, we compared kymographs of N-C dynamics. In *+/y* neurons, we found that following a peak in the N-C distance, about 1/3 of the time the nucleus immediately translocated towards the centrosome, whereas nuclear translocation occurred much less frequently in *-/y* neurons (Fig. 4e). In these *-/y* neurons, typically the centrosome fell back towards the nucleus following an N-C peak, rather than the nucleus translocating towards the centrosome. This effect was quantitated by measuring the number of nuclear translocation (NT) events (defined as nuclear movements greater than 3 μm distance) per number of N-C peaks (defined as maximum N-C distance in two consecutive time points) in *+/y* and *-/y* neurons. NT events occur half as frequently in *-/y* neurons compared with *+/y* following a N-C peak (Fig. 4f). We conclude that there is a defect in nuclear translocation towards the centrosome but not centrosome positioning in *Dcx -/y* neurons.

DCX functions in suppression of branching of the primary neurite

We next tested for a defect in the first phase of neuronal migration: Leading process extension. We found a striking defect in both the length of the leading process and in the frequency of cells with secondary neurite branches, suggesting a defect in neurite stabilization or organization in the absence of *Dcx*. The average length of the leading process of *Dcx -/y* neurons was 30% shorter than *+/y* neurons (Fig. 5a, b). We tested whether there was a difference in the number of cells with simple bipolar shape vs. branched leading processes, because this was identified as a possible defect following siRNA treatment to knockdown Dcx [50] and we observed this frequently in RMS slices from knockouts (see Fig. 3a). A secondary branch was defined as a protrusion from either the primary neurite or the cell body that was at least 1 somal length and more than

1 somal length removed from the tip of the growth cone (to differentiate these from branched growth cones). There was a dramatic increase in the average number of secondary branches per cell, where *-/y* neurons displayed twice as many secondary branches, on average, over the course of the analysis. These secondary branches either extended from the cell body adjacent to the primary neurite, or from the base of the primary neurite (Fig. 5a,c). We questioned whether these secondary branches might relate to the migration defect, so we compared the average number of secondary branches per cell per frame with average migration velocity in a cohort of *Dcx* -/y neurons. There was a clear negative correlation, as cells with fewer secondary neurite branches displayed more rapid rates of migration (Fig. 5d). We conclude that *Dcx* is required for maintenance of bipolar shape during migration.

Nuclear translocation defect likely secondary to leading process branching phenotype

We questioned whether the defect in nuclear translocation might be secondary to the defect in neuronal morphology, since it was possible that slowed migration could lead to excessive branching. To address this issue, we repeated the nuclear translocation experiments but this time captured high-resolution phase images in one microscopy channel in addition to the nuclear and centrosome channels in timelapse analysis. We tested the frequency of nuclear translocation (NT) events per N-C peak in both *wt* and mutant cells, and grouped them based on whether the cells had a single or multiple processes. In *wt* cells with a single leading process, an NT event occurred at approximately 50% of the N-C peaks (Fig. 5e). In rare *wt* cells with more than one branch (defined as a branched process greater than one cell-body in length), NT events occurred at approximately 20% of the N-C peaks. This data indicates that branched neurons are less likely to show NT events following N-C peaks, and suggested that the nuclear translocation defect we observed in *Dcx -/y* neurons may be secondary to the increased number of branched neurons. To test this we performed the same analysis in *Dcx -/y* neurons. We found that there were fewer NT events per N-C peak in cells with single processes from *-/y* compared with *+/y* neurons. Even more striking, however was that *-/y* neurons with multiple processes showed many fewer NT events per N-C peak

than those with single processes. This data suggests that the *Dcx* is required for suppression of multiple branching, and that this branching defect may lead to the NT defect we observed.

DISCUSSION

In this study, we show that the microtubule-associated protein DCX is expressed by tangentially migrating neuroblasts in the RMS. We found that *Dcx* inactivation correlated with a phenotype of disrupted neuronal migration in this location. This result was surprising given the lack of other clear evidence of disrupted migration associated with this mouse mutation, but not completely unexpected given the strong migration defect displayed by humans with mutations. As a result, we observed a reduction in the number of neurons that achieve correct final positioning. The neurons in this mutant fail to achieve proper velocity, but display no defect in direction of migration or response to guidance cues. In these neurons, DCX functions in suppression of secondary branching of the leading neurite, and in translocation of the nucleus in the direction of migration. These findings imply that DCX plays a critical role in the adult forebrain in maintaining bipolar morphology and in nuclear translocation during neuroblast migration.

Role of Dcx in the RMS

The two primary zones of adult proliferation are the subgranular layer of the hippocampal dentate gyrus and the SVZ of the forebrain, although other zones are also thought to exist [51, 52]. DCX has become a widely used marker for newly generated neuroblasts in proliferative zones in adult [14, 31, 53, 54]. In these regions, DCX is expressed exclusive of GFAP positive cells, and appears to be one of the earliest markers for cells transitioning from astrocytic glia to neuroblasts in the SVZ and RMS [32].

To identify a potential role for DCX in adult neurogenesis, we tested for alteration following deletion. Our findings suggest that DCX is required for cell migration through the RMS. Loss of *Dcx* resulted in changes in morphology of the RMS, characterized by a widened collection of neuroblasts and glia with altered orientation within the stream, presumably a result of slowed migration of neurons that are ahead of them in the neuroblast chain. This may lead to a blockage of neuronal migration in the RMS that is

partially cell-autonomous and partially non-cell autonomous. As DCX is clearly not expressed in glia of the RMS, the increase in number of glia and malorientation of these cells relative to the direction of the RMS may reflect glial proliferation in response to stalled neuronal migration, as has been reported in the NCAM mutant resulting in a similar phenotype [22].

BrdU labeling indicated slowed migration through the RMS, with many cells maintaining a position within the widened RMS in the week subsequent to the injection. Normally, cells transition from the SVZa to the OB over a 2-week window. Because the overall number of BrdU positive neurons was not appreciably different in *Dcx +/y* and *-/y* brains, there is unlikely to be a major difference in cell proliferation as a result of defective migration. These stalled neuroblasts appear to take on one of several fates, as we found evidence of increased differentiated neurons and apoptosing cells in the RMS. Live cell imaging from acute brain slices showed slowing of migration that was independent of direction of migration or cell orientation. This suggests the role of Dcx is in mediating cell movement, rather than transducing extracellular guidance cues or determining cell directionality. The loss of *Dcx* also affected neuroblast migration *in vitro*, as SVZ explants prepared from *Dcx -/y* had reduced ability to migrate in a collagen/Matrigel matrix. Together, these observations provide evidence that DCX activity is required for RMS neuronal migration.

Other gene defects resulting from defective neuronal migration also display morphological defects in the RMS. Mutations in the transcriptional regulator *Arx* (*Aristaless related homeobox*), a gene required for neocortical development, and *NCAM*, encoding a cell adhesion molecule, among others lead to disrupted RMS migration and reduced olfactory bulb size [22, 55]. This may be a result of failure of adult-generated SVZa neurons to deposit within the OB, or may reflect an earlier requirement for these genes on development. We found only a modest reduction in OB size in the *Dcx* mutant that was not statistically significant (not shown). The results from several studies have indicated that disrupted migration results in reduced numbers of GABAergic neurons in the OB, although the functional implication of these alterations have not been thoroughly tested. We performed electrophysiological assessment of glomerular physiology and failed to identify a striking difference in GABAergic potentials in *Dcx +/y* and *-/y* littermates (data

not shown). This might relate to the relatively small number of newly generated neurons that survive long-term in the OB, or compensatory increase in the amount of GABA released from cells.

Controversies about the role of DCX in brain development across evolution

The *Dcx* knockout mouse, which should be a genetic equivalent of humans with *DCX* mutations, displays normal neocortical migration with poorly laminated hippocampal CA neurons as the only other migration phenotype [28]. However, inactivation with RNAi mediated gene-silencing results in a defect in migration in the neocortex in rat and mouse [50], which is largely but not exclusively cell autonomous. One theory that explains these differences is that germline gene knockout may activate some compensatory mechanism or alternative migration mode that is not induced following acute inactivation with RNAi [56].

Our results provide the first evidence that germline inactivation of *Dcx* in rodent results in demonstrable defects in neuronal migration. The question remains as to why germline inactivation does not disrupt neocortical migration in mouse, as there is such a profound defect in human with mutations. Possible explanations include: 1. Human mutations, representing mostly mid- or late-truncations or missense mutations [57], may be fundamentally different, perhaps displaying dominant effects. 2. Humans and mice may utilize different modes of migration in the neocortex. 3. The greater distance neurons migrate in human (as a result of a larger cerebral cortex). 4. Compensatory genetic mechanisms, which have been recently described with *doublecortin-like kinase* [58, 59]). The reason a migration phenotype exists in the RMS but not in neocortex in mouse may similarly relate to any of these possibilities.

DCX as a regulator of radial and tangential migration

RNAi-mediated knockdown of *Dcx* introduced by electroporation of constructs into the lateral ventricle resulted in impaired migration, which likely reflects radially migrating neurons [50]. Our results demonstrate a requirement for DCX in neuronal migration in the RMS, which migrate tangentially [15]. The distinction between radial and tangential migration may be blurred somewhat in the RMS, as neurons undergo chain migration but

through a substrate of glial guidance. A similar requirement for LIS1 and components of the reelin pathway in both radial and tangential migration have reported [18, 60-62].

DCX plays an essential role in translocation of the nucleus

We identified a requirement for DCX in mediating coupling between the nucleus and the centrosome during neuronal migration in SVZa derived neurons. The centrosome is an organelle best known for its role in mitosis. It serves as the microtubule-organizing center, and most microtubules emanate from the centrosome. Microtubules are intrinsically polarized, and grow exclusively from the "plus" end. The centrosome serves to anchor the "minus" end of microtubules, where they are nucleated through a combined effect of pericentrosomal proteins including γ-tubulin. Notably, we found no defect in centrosome number or morphology in *Dcx -/y* neurons, based on immunofluorescence of pericentrin and centrin (Supplemental Fig. 6).

During neuronal migration, the centrosome of the cell is uniformly positioned in front of the nucleus [63-65], leading to a model in which the nucleus is translocated along microtubules in the "minus" direction through "minus"-end directed motors including dynein. Indeed, disruption of dynein function, or alterations in LIS1 or Ndel1, which are dynein components, similarly lead to alterations in this coupling, as measured by an increased distance between the nucleus and centrosome (i.e. coupling) [45, 46]. It was previously demonstrated that overexpression of DCX led to an amelioration of the migration defects in *Lis1 +/-* neurons and corrected the nuclear-centrosome coupling defect [45]. We now show that deletion of *Dcx* leads to a defect in nuclear translocation that was not evident by measurement of N-C coupling alone. As DCX is a potent microtubule-associated protein and localized prominently to perinuclear microtubules [31, 43], we hypothesize that it is required for formation or stabilization of these microtubules, or in mediating transport of the nucleus along these microtubules, possibly in association with the LIS1/Ndel1/dynein complex.

DCX plays an essential role in maintaining bipolar morphology

We found that neurites from *Dcx* -/y neurons were shorter and more highly branched. A similar branched phenotype was reported in migrating neurons in the cortex of the *p35*

mutant [66], where it was thought to contribute to altered cortical lamination. Since p35/CDK5 complex interacts with DCX, it is possible that this interaction relates to the branched phenotype [67]. What could the role of DCX be in maintaining this bipolar morphology? We excluded a defect in transducing guidance cues, as reversal of polarity in response to Slit was normal. Altered microtubule dynamics was considered as a possibility, but we excluded an obvious defect in microtubule plus-end dynamics as measured by the rate of movement of EB1-positive punctae (Supplemental Fig. 7). We also excluded an obvious defect in the rate of neurite retraction/extension following application and washout of the microtubule depolymerizing agent nocodazole in *Dcx -/y* neurons (Supplemental Fig. 8), arguing against a major defect in microtubule growth. However, these tests do not evaluate for defects in microtubule bundling. Our preliminary data suggest a defect in microtubule cross-linking and bundling in stationary neurons (data not shown), arguing that such a defect may underlie the branched morphology phenotype that results in the mutant.

Our data suggest that the branched phenotype we observed may at least partly be responsible for the difference in NT events in *Dcx -/y* neurons. We found that cells with branched morphology had fewer NT events per N-C peak, irrespective of *Dcx* genotype. The fact that the branched phenotype was more common in *Dcx -/y* neurons may therefore account for the failure in migration. Recent evidence suggests that SVZa neurons may use branching as a means of changing migration direction, and cells with branched morphology typically stabilized a dominant process and withdrew the secondary process before initiating nuclear movement [68]. Therefore, NT and cell morphology appear to be temporally related, and further work into this connection is warranted.

METHODS

Histochemistry. Antibodies to DCX (C-terminal polyclonal, Santa Cruz), and PSA-NCAM, NeuN, Active caspase-3, tyrosine hydroxylase (Chemicon), TuJ1, Pericentrin (Covance), Calbindin D-28K, Parvalbumin (Sigma), Calretinin (Swant), Centrin2 (gift of J. Salisbury, Mayo Clinic) were used as described previously [31].

Mice. Mice were cared for in accordance with animal protocols approved by the University of California, San Diego. The *Dcx* +/- mice were maintained on a mixed genetic background composed of C57/Bl6 and 129SVJ [28]. GFP-CETN2 mice were maintained on a mixed background composed C57/Bl6 and BalbC [49]. The *Dcx::EGFP* mice originated on a FVB/N;Swiss Webster line. All experiments were performed on experimental and *wt* littermates. BrdU labeling was performed with 0.1 mg/g BrdU and detected with anti-BrdU (Becton Dickinson), 1:100, and Vector ABC detection system (Vector Laboratories).

Acute slice preparation. Mice were genotyped at P5. Uniform parasagittal 300 μm brain sections (MX-TS Tissue Slicer) were mounted in a 1:1 collagen /culture media mixture, stabilized for several hours, then subject to multiphoton microscopy. DiI labeling was performed as reported [39], except that after 12-hour incubation, slices immobilized in collagen gel and subject to multiphoton microscopy.

SVZa explants. This assay was carried out as reported [17]. Slit 2 was applied as conditioned media [69] to explants. As Slit diffuses through the collagen-Matrigel matrix, neurons respond by repolarizing and reversing migration direction back towards the explant [39]. Nocodazole was added at 1-3 μg/ ml. Neurite length was determined using the SoftWorx software package from Applied Precision.

Microscopy. Confocal images were acquired using an Olympus FV1000 system. Multiphoton live cell acute slice imaging was performed using an Olympus FV300 upright microscope with a Coherent MaiTai laser and with temperature and CO_2 incubation at an excitation of 900 nM. Images were acquired with a *z*-step of 2 μm and depth of 100 μm through the RMS. Cell tracking was performed with ImageProPlus (Media Cybernetics). Fluorescent and DIC live cell migration imaging of SVZ explants was performed with a DeltaVision deconvolution system with temperature and CO_2 incubation using multipoint revisiting, a *z*-step of 2 μm.

Lentivirus production. EB1 [70] was cloned into pLentiLox 3.7 [71] by first removing the EGFP of pLentiLox, then ligation of the full-length EB1-GFP. High-titer viral particles were obtained as described [72], then incubated with RMS explants for 30 hours. Explants were plated for additional 18 hours prior to imaging.

FIGURE LEGENDS

Figure 1. Abnormally thickened RMS in *Dcx* -/y mutant mice. (**a, b)** Cresyl violet stained matching parasagittal sections from adult *Dcx +/y* and *-/y* littermates. Note the thickened appearance of the RMS, especially at the central region (double arrows). (**c, d)** Matching coronal sections from the rostral forebrain from *Dcx +/y* and *-/y* littermates. The RMS was visible in dark blue, outlined by perpendicular arrows, and was significantly greater in size in mutants. (**e, f)** Thickened RMS in mutant consists of PSA-NCAM and GFAP positive cells. Scale bar 100 μm. (**g, h)** High-power view of RMS co-stained for TuJ1 and GFAP. In *Dcx +/y* there is an orderly appearance of the migratory TuJ1 (+) neurons and GFAP (+) glia, with uniform orientation in the direction of migration (indicated by white arrow). In *Dcx -/y*, the close approximation of TuJ1 and GFAP (+) cells was maintained, but the cell orientation was less ordered (arrowheads indicate GFAP (+) cells of non-uniform orientation). Scale bar 100 μm. (**i, j)** Increased number of NeuN (+) (red nuclei) differentiated neurons in *Dcx -/y* RMS. RMS defined by *Dcx::EGFP* signal. Scale bar 50 μm. (**k, l)** Increased number of activated caspase-3 (CAS3) (+) cells. Note cells in *Dcx -/y* (arrows) within the limits of the RMS (white lines) that are not apparent in *Dcx +/y*. Scale bar 100 μm.

Figure 2. Newly generated neurons fail to migrate properly in *Dcx* -/y mice. (**a, b)** BrdU was administered at P28 and brains harvested at P35. Appearance of BrdU labeled neurons (black signal, highlighted by arrows) in the SVZa in *Dcx +/y* and *-/y* are indistinguishable. Anterior edge of ventricle outlined by dash. Scale bar 200 μm. (**c, d)** Failure of BrdU labeled neurons to transverse the SVZa. In *Dcx +/y*, BrdU labeled cells are visible in the thin stream of the RMS (large arrow), where they fan out in the proximal OB (double arrows), and in the granule cell layer (small arrows). In the mutant, many BrdU positive neurons are visible in the proximal RMS (large arrow), a lesser number are visible in rostral RMS (double arrows) and very few are visible in the granule cell layer (*). Scale bar 600 μm. (**e, f)** BrdU was administered at P28 and brains harvested at P56. BrdU labeled neurons (brown, highlighted by arrows) in glomerular layer are less numerous in the mutant. (**g**) Quantitation of BrdU+ cell numbers in GL (e-f, normalized to standard area) shows about a 50% decrease. Three serial matched

sections from n =3 mice for each genotype. * $p < 0.01$ Student t-test. (**h, j)** Decreased number of calbindin positive cells per glomerulus in 50 µm sections in the *Dcx* -/y mutant. Glomeruli outlined by black circles. Note decreased number of brown cells in mutant (arrows). Quantification from serial sections shows significant decrease in positive cells. $n > 30$ glomeruli from each of three mice of each genotype from matched sections. Error bar = S.E.M. * $p < 0.01$, Student t-test. Abbreviations GL = glomerular layer, EPL = external plexiform layer, GC = granule cell layer.

Figure 3. Defect in average velocity reflects "stutter" in migration initiation in *Dcx* -/y slices. (**a)** DiI labeled RMS slices showing multiphoton images from *Dcx +/y* and -/y live brain slices through the RMS. The *wt* cell is shown moving towards the OB at a steady rate, with regular advances of the leading process (arrowhead) followed by movement of the soma (arrow). In the mutant, there is excessive branched morphology (arrowheads) and the cell soma does not move well. OB is to right, time in min. Scale bar = 50 µm. (**b)** Fluorescent image of GFP signal from *Dcx::EGFP* transgenic mouse, showing endogenous GFP signal along the RMS (arrowhead). Scale bar = 500 µm. (**c)** x-y-t maximum-z projection tracing showing starting point (large colored circle) and migration steps (5 min intervals). Note steady rate of movement in most cells in *wt* whereas mutant shows frequent long stuttering (arrows). (**d, e)** Defective average and ranked velocity in mutant neurons. n = 53 *wt* and 44 mutant neurons traced over 10 hours from 300 µm z-axis image stack acquired every 5 min. Both average and ranked velocity was significantly decreased (Student t-test and Kruskal-Wallis Rank-sum-test, respectively, * $p < 0.01$). Error bar = S.E.M. (**f)** No alteration in direction of migration in mutant slices. Approximately the same percent of cells showed net displacement towards or away from bulb during the 6-hour recording. **(g)** No alteration in the ranked maximum velocity for each cell, showing similarly shaped curves and no statistical differences ($p > 0.05$, Student t-test). For (c-g) only cells that moved at least one cell-body length during the experiment were tracked.

Figure 4. Decreased migration of neurons exiting SVZa due to a defect in nuclear translocation events. (**a)** Explant culture of SVZa in collagen/Matrigel matrix shows

severely impaired neuronal migration in *Dcx -/y* following 16-hour incubation period. Scale bar = 100 μm. (**b)** Significant decrease in average migration in *Dcx -/y* mutants, calculated as distance neurons migrated from edge of reaggregates in a fixed time. $n > 22$ explants and 1200 cells for each genotype, * $p < 0.01$, Student *t*-test, summed from three experiments). (**c)** Significant decrease in the average migration velocity measured in μm/min from 2-hour movies from over 100 neurons of each genotype. * $p < 0.01$, Student *t*-test. Summed from three experiments. (**d)** Average nuclear-centrosome distance is not altered in *Dcx -/y* neurons. $n = 111$ wt and 76 mutant neurons, respectively. Distance between centrosome and leading edge of nuclear membrane is in μm. $n = 30$ neurons with 40 frames/neuron, for each genotype, $p > 0.05$, Student *t*-test (**e)** Kymograph of *wt* and mutant nuclear-centrosome dynamics. Initial nuclear position is shown by bracket and initial centrosome position shown by green arrow (1). In *wt*, following a peak in the N-C distance (P bracket) there is an abrupt nuclear translocation event (<) within 10 min. The (2) bracket and arrow represent the new positions. In mutant, there are two N-C distance peaks (P bracket) and neither is followed by nuclear translocation. Each frame 3.5 min. (**f)** Decreased nuclear translocation (NT) events per N-C distance peak in mutant (see text for definitions). In *wt*, N-C distance peaks led to a NT event approximately 37% of the time, whereas this occurred 25% of the time in mutant. $n = 85$ events, total of 15 neurons from each genotype. Error bar = S.E.M.

Figure 5. DCX functions in suppression of branching of the primary neurite. (a) Isolated neuron showing typical bipolar morphology of *Dcx +/y* neuron and typically highly branched morphology of *-/y* neurons. Excessive branches were evident from both proximal (arrow) and distal (arrowhead) segments of neurite. GFP-labeled centrosome is evident (green, arrow). Supplemental Movies 3-4 demonstrate typical migration of these cells. (**b)** Average leading process length (measured as a line from the base to the tip of the process) was decreased by approximately 30% in mutant. Average 32 μm vs. 22 μm, $n > 100$ each genotype, * $p < 0.01$ Student *t*-test. (**c)** Average number of secondary branches was determined as a function of time in migrating neurons. A striking increase in the average number of secondary branches was noted in the mutant. Each frame 7.5 min, $n = 109$ wt and 52 mutant cells, * $p < 0.01$, Student *t*-test. (**d)** Strong inverse

correlation between average migration velocity (ranked in decreasing order) vs. average number of secondary branches per cell per frame. Total 16 frames of 15 min interval. (**e)** Nuclear translocation events per N-C peak is significantly reduced in neurons with multiple processes compared to those with single processes, in both *+/y* and *-/y* neurons. Error bar = S.E.M.

Supplemental Figure 1. Co-distribution of Dcx with markers of migration within the SVZa and RMS in postnatal mice. (**a-c)** Co-distribution of Dcx and PSA-NCAM in the SVZa/RMS (arrows) and proximal olfactory bulb (asterisk). There was a thin stream of cells expressing both Dcx and PSA-NCAM that expanded over the caudal-rostral dimension of the bulb. (**d, e)** Co-distribution of Dcx with PSA-NCAM and TuJ1 in cells within the chains of the RMS (arrows). Scale bar (a) 2mm, (d, e) 150 μm.

Supplemental Figure 2. Abnormally thickened RMS in *Dcx -/y* mice as analyzed by serial section. Top and bottom panels show every third 50 μm sections from the rostral to caudal RMS in 7-week old *Dcx +/y* and *-/y* mice. Note that the large dark blue region of the RMS (*****) is significantly larger in sections through the mutant.

Supplemental Figure 3. RMS defect is fully expressive in *Dcx -/-* but not +/- female mice. (a-f) Cresyl violet-staining showing adult *+/y* males, +/- females and *-/y* males. Note that the RMS in the +/- female is not different in appearance from +/y males (arrows). (**g-i)** Thickened RMS in -/- female is indistinguishable from *-/y* male (arrow).

Supplemental Figure 4. No significant difference in numbers of calretinin (CR), parvalbumin (PV) or tyrosine hydroxylase (TH)-positive cells in the glomerular layer of *Dcx -/y* mice. (**a, b)** Sections from adult mice show roughly equal numbers of positive neurons (arrows) per glomerulus (circles). (**d, e, g, h)** PV and TH positive neurons (arrows) are visible surrounding glomeruli, and no significant differences in numbers of labeled cells per normalized area were apparent. (**c, f, i)** Quantification shows slightly lower positive cells in mutant GL for each, but differences were not statistically significant. (c) $n > 30$ glomeruli from each of three mice of each genotype from matched

sections. (f, i) 3 serial matched sections from *n* =3 mice for each genotype. Error bar = S.E.M. GL = glomerular layer, EPL = external plexiform layer, GC = granule cell layer.

Supplemental Figure 5. No apparent defect in responsiveness of *Dcx -/y* neurons to Slit chemorepulsion. (a) Method for testing effect of Slit on neuronal reorientation. Explants were cultured in a collagen-Matrigel matrix for 12 hours, to allow neurons to exit and begin migration, followed by bath application of Slit. Most cells reorient and migrate back into the explant in the subsequent 2 hours. (**b, c)** Mutant *Dcx -/y* neurons have no apparent defect in re-polarization in response to Slit chemorepulsion. Neuronal morphology in *Dcx +/y* (left) and *-/y* (right) neurons before Slit application oriented away from explant (outlined in black) with leading process (arrow) in front of cell soma (arrowhead). Following Slit application neuronal repolarization is evident in *Dcx -/y* and *+/y*, with leading process oriented back towards the explant. Scale bar 50 μm. (**d)** No significant difference in proportion of neurons from explants that repolarize in response to Slit. *n* = 169 wt and 83 mutant cells imaged for 2 hours following Slit application, $p > 0.05$, Student *t*-test. Error bar = S.E.M.

Supplemental Figure 6. No apparent defect in appearance of the centrosome in *Dcx -/y* neurons. Dissociated migrating SVZa neurons were fixed and stained for centrosomal markers. Note the pair of centrioles seen with centrin labeling (green, pair of arrows) and the pericentriolar matrix seen with pericentrin labeling (red, arrowhead). Hoechst stain (blue) shows nucleus. Scale bar 5 μm.

Supplemental Figure 7. No apparent defect in plus-end microtubule dynamics in *Dcx* -/y neurons. Migrating SVZa neurons were infected with a lentivirus encoding End-Binding protein 1 (EB1)-tagged GFP. By 48 hours, distinct punctate signals were observed in the leading process (top, arrowhead), and could be observed in timelapse analysis to move towards the growth cone (arrow). Timelapse analysis of each punctum for 2 hour (every 10 sec) from 10 cells of each genotype (total $n > 240$ from each genotype) showed no significant difference in this movement. Error bar = S.E.M.

Supplemental Figure 8. No difference in leading process retraction or growth following acute application then washout of the microtubule depolymerizing agent nocodazole. Nocodazole (1-3 μg/ml) was added at time zero, and timelapse analysis was obtained for 50 min (every 5 min) to capture rate of process retraction. Subsequently, the drug was washed out and timelapse analysis for 3-hours (every 5 min) to capture rate of process re-extension. No significant differences were noted. *n* = 33 *wt* and 61 mutant cells. Averaged from 2 trials. Error bar = S.E.M.

Supplemental Movie 1, 2.

Time lapse imaging of neuronal movement from *Dcx +/y; Dcx::EGFP* (Movie 1) and *Dcx -/y; Dcx::EGFP* (Movie 2). Compressed image stack from 4-hour acquisition, 300 μm *z*-axis image stack acquired every 5 min shown at same magnification. In *wt*, note rapid movement of GFP-positive cells, whereas mutant shows many more GFP-positive cells, frequent multipolar morphology, and frequent oscillating "stutter"-like movements with most cells failing to show significant migration.

Supplemental Movie 3, 4.

Time lapse DIC and fluorescent imaging of *Dcx -/y; βactin::Cetn2-EGFP* and *Dcx* +/y; *βactin::Cetn2-EGFP* isolated neurons in gel matrix. Images acquired every 7.5 min. Cell body outlined in white, green signal shows centrosome (arrow). In *wt* (Movie 3) there is leading process extension, followed by advancement of the centrosome into the leading process, followed by translocation of the nucleus towards the leading process. In mutant (Movie 4), the leading process remains highly branched throughout the image series, and there is little nuclear translocation.

ACKNOWLEDGEMENTS

The authors wish to thank Dr. Anthony Wynshaw-Boris and Christopher A. Walsh for *Dcx* knockout mice, Mary E. Hatten and Nathanial Heitz (Rockefeller University, http:www.gensat.org; NIH NS02331) and Juergen Winkler and Ludwig Aigner (University of Regensburg) for *Dcx::EGFP* mice, Michael Ward and Yi Rao (Northwestern University) for help with SVZa explant culture system and Slit-producing stable HEK293T cell line, the Tsukita lab (Japan Science and Technology Corporation) for the GFP-EB1 clone, Niels Bjarne Woods and Robert Marr of the Inder Verma lab (Salk Institute) for lentiviral vectors and assistance, and Jeffrey Isaacson (UCSD) for electrophysiological measurements. This work was funded by the NINDS (R01 NS04387 and NS47101). We thank the UCSD Neurosciences Microscopy Shared Facility for imaging support.

REFERENCES

1. Altman, J. Autoradiographic and histological studies of postnatal neurogenesis. IV. Cell proliferation and migration in the anterior forebrain, with special reference to persisting neurogenesis in the olfactory bulb. J Comp Neurol 137, 433-57 (1969).
2. Bayer, S. A. 3H-thymidine-radiographic studies of neurogenesis in the rat olfactory bulb. Exp Brain Res 50, 329-40 (1983).
3. Lois, C. & Alvarez-Buylla, A. Proliferating subventricular zone cells in the adult mammalian forebrain can differentiate into neurons and glia. Proc Natl Acad Sci U S A 90, 2074-7 (1993).
4. Luskin, M. B. Restricted proliferation and migration of postnatally generated neurons derived from the forebrain subventricular zone. Neuron 11, 173-189 (1993).
5. Altman, J. & Das, G. D. Autoradiographic and histological evidence of postnatal hippocampal neurogenesis in rats. J Comp Neurol 124, 319-35 (1965).
6. Eriksson, P. S. et al. Neurogenesis in the adult human hippocampus. Nat Med 4, 1313-7 (1998).
7. Kornack, D. R. & Rakic, P. Continuation of neurogenesis in the hippocampus of the adult macaque monkey. Proc Natl Acad Sci U S A 96, 5768-73 (1999).
8. van Praag, H. et al. Functional neurogenesis in the adult hippocampus. Nature 415, 1030-4 (2002).
9. Belluzzi, O., Benedusi, M., Ackman, J. & LoTurco, J. J. Electrophysiological differentiation of new neurons in the olfactory bulb. J Neurosci 23, 10411-8 (2003).
10. Liu, S. et al. Generation of functional inhibitory neurons in the adult rat hippocampus. J Neurosci 23, 732-6 (2003).
11. Benninger, F. et al. Functional integration of embryonic stem cell-derived neurons in hippocampal slice cultures. J Neurosci 23, 7075-83 (2003).
12. Lois, C., Garcia-Verdugo, J. M. & Alvarez-Buylla, A. Chain migration of neuronal precursors. Science 271, 978-81 (1996).
13. Doetsch, F., Caille, I., Lim, D. A., Garcia-Verdugo, J. M. & Alvarez-Buylla, A. Subventricular zone astrocytes are neural stem cells in the adult mammalian brain. Cell 97, 703-16 (1999).
14. Garcia, A. D., Doan, N. B., Imura, T., Bush, T. G. & Sofroniew, M. V. GFAP-expressing progenitors are the principal source of constitutive neurogenesis in adult mouse forebrain. Nat Neurosci 7, 1233-41 (2004).
15. Doetsch, F. & Alvarez-Buylla, A. Network of tangential pathways for neuronal migration in adult mammalian brain. Proc Natl Acad Sci U S A 93, 14895-900 (1996).
16. Nguyen-Ba-Charvet, K. T. et al. Multiple roles for slits in the control of cell migration in the rostral migratory stream. J Neurosci 24, 1497-506 (2004).
17. Wu, W. et al. Directional guidance of neuronal migration in the olfactory system by the protein Slit. Nature 400, 331-6 (1999).

18. Hack, I., Bancila, M., Loulier, K., Carroll, P. & Cremer, H. Reelin is a detachment signal in tangential chain-migration during postnatal neurogenesis. Nat Neurosci 5, 939-45 (2002).
19. Hu, H. Chemorepulsion of neuronal migration by Slit2 in the developing mammalian forebrain. Neuron 23, 703-11 (1999).
20. Anton, E. S. et al. Receptor tyrosine kinase ErbB4 modulates neuroblast migration and placement in the adult forebrain. Nat Neurosci 7, 1319-28 (2004).
21. Murase, S. & Horwitz, A. F. Deleted in colorectal carcinoma and differentially expressed integrins mediate the directional migration of neural precursors in the rostral migratory stream. J Neurosci 22, 3568-79 (2002).
22. Chazal, G., Durbec, P., Jankovski, A., Rougon, G. & Cremer, H. Consequences of neural cell adhesion molecule deficiency on cell migration in the rostral migratory stream of the mouse. J Neurosci 20, 1446-57 (2000).
23. Hu, H., Tomasiewicz, H., Magnuson, T. & Rutishauser, U. The role of polysialic acid in migration of olfactory bulb interneuron precursors in the subventricular zone. Neuron 16, 735-43 (1996).
24. Petreanu, L. & Alvarez-Buylla, A. Maturation and death of adult-born olfactory bulb granule neurons: role of olfaction. J Neurosci 22, 6106-13 (2002).
25. Winner, B., Cooper-Kuhn, C. M., Aigner, R., Winkler, J. & Kuhn, H. G. Long-term survival and cell death of newly generated neurons in the adult rat olfactory bulb. Eur J Neurosci 16, 1681-9 (2002).
26. Gleeson, J. G. et al. *doublecortin,* a brain-specific gene mutated in human X-linked lissencephaly and double cortex syndrome, encodes a putative signaling protein. Cell 92, 63-72 (1998).
27. des Portes, V. et al. doublecortin is the major gene causing X-linked subcortical laminar heterotopia (SCLH). Hum Mol Genet 7, 1063-70 (1998).
28. Corbo, J. C. et al. Doublecortin Is required in mice for lamination of the hippocampus but not the neocortex. J. Neurosci. 22, 7548-7557 (2002).
29. Letinic, K., Zoncu, R. & Rakic, P. Origin of GABAergic neurons in the human neocortex. Nature 417, 645-9 (2002).
30. Nacher, J., Crespo, C. & McEwen, B. S. Doublecortin expression in the adult rat telencephalon. Eur J Neurosci 14, 629-44 (2001).
31. Gleeson, J. G., Lin, P. T., Flanagan, L. A. & Walsh, C. A. Doublecortin is a microtubule-associated protein and is expressed widely by migrating neurons. Neuron 23, 257-71 (1999).
32. Brown, J. P. et al. Transient expression of doublecortin during adult neurogenesis. J Comp Neurol 467, 1-10 (2003).
33. Rousselot, P., Lois, C. & Alvarez-Buylla, A. Embryonic (PSA) N-CAM reveals chains of migrating neuroblasts between the lateral ventricle and the olfactory bulb of adult mice. J Comp Neurol 351, 51-61 (1995).
34. Bedard, A., Levesque, M., Bernier, P. J. & Parent, A. The rostral migratory stream in adult squirrel monkeys: contribution of new neurons to the olfactory tubercle and involvement of the antiapoptotic protein Bcl-2. Eur J Neurosci 16, 1917-24 (2002).

35. Kosaka, K. et al. Chemically defined neuron groups and their subpopulations in the glomerular layer of the rat main olfactory bulb. Neurosci Res 23, 73-88 (1995).
36. Brinon, J. G. et al. Calbindin D-28k-positive neurons in the rat olfactory bulb. An immunohistochemical study. Cell Tissue Res 269, 289-97 (1992).
37. Gong, S. et al. A gene expression atlas of the central nervous system based on bacterial artificial chromosomes. Nature 425, 917-25 (2003).
38. Mainen, Z. F. et al. Two-photon imaging in living brain slices. Methods 18, 231-9, 181 (1999).
39. Ward, M., McCann, C., DeWulf, M., Wu, J. Y. & Rao, Y. Distinguishing between directional guidance and motility regulation in neuronal migration. J Neurosci 23, 5170-7 (2003).
40. Martinez-Lopez, M. J. et al. Mouse Neuron navigator 1, a novel microtubule-associated protein involved in neuronal migration. Mol Cell Neurosci 28, 599-612 (2005).
41. Del Rio, J. A. et al. MAP1B is required for Netrin 1 signaling in neuronal migration and axonal guidance. Curr Biol 14, 840-50 (2004).
42. Tsai, L. H. & Gleeson, J. G. Nucleokinesis in neuronal migration. Neuron 46, 383-8 (2005).
43. Francis, F. et al. Doublecortin is a developmentally regulated, microtubule-associated protein expressed in migrating and differentiating neurons. Neuron 23, 247-56 (1999).
44. Friocourt, G. et al. Doublecortin functions at the extremities of growing neuronal processes. Cereb Cortex 13, 620-6 (2003).
45. Tanaka, T. et al. Lis1 and doublecortin function with dynein to mediate coupling of the nucleus to the centrosome in neuronal migration. J Cell Biol 165, 709-21 (2004).
46. Shu, T. et al. Ndel1 operates in a common pathway with LIS1 and cytoplasmic dynein to regulate cortical neuronal positioning. Neuron 44, 263-77 (2004).
47. Kamiya, A. et al. A schizophrenia-associated mutation of DISC1 perturbs cerebral cortex development. Nat Cell Biol 7, 1167-78 (2005).
48. Solecki, D. J., Model, L., Gaetz, J., Kapoor, T. M. & Hatten, M. E. Par6alpha signaling controls glial-guided neuronal migration. Nat Neurosci 7, 1195-203 (2004).
49. Higginbotham, H., Bielas, S., Tanaka, T. & Gleeson, J. G. Transgenic mouse line with green-fluorescent protein-labeled Centrin 2 allows visualization of the centrosome in living cells. Transgenic Res 13, 155-64 (2004).
50. Bai, J. et al. RNAi reveals doublecortin is required for radial migration in rat neocortex. Nat Neurosci 6, 1277-83 (2003).
51. Dayer, A. G., Cleaver, K. M., Abouantoun, T. & Cameron, H. A. New GABAergic interneurons in the adult neocortex and striatum are generated from different precursors. J Cell Biol 168, 415-27 (2005).
52. Magavi, S. S., Leavitt, B. R. & Macklis, J. D. Induction of neurogenesis in the neocortex of adult mice. Nature 405, 951-5 (2000).
53. Jin, K. et al. Vascular endothelial growth factor (VEGF) stimulates neurogenesis in vitro and in vivo. Proc Natl Acad Sci U S A 99, 11946-50 (2002).

54. Bedard, A. & Parent, A. Evidence of newly generated neurons in the human olfactory bulb. Brain Res Dev Brain Res 151, 159-68 (2004).
55. Yoshihara, S., Omichi, K., Yanazawa, M., Kitamura, K. & Yoshihara, Y. Arx homeobox gene is essential for development of mouse olfactory system. Development 132, 751-62 (2005).
56. Gotz, M. Doublecortin finds its place. Nat Neurosci 6, 1245-7 (2003).
57. Matsumoto, N. et al. Mutation analysis of the DCX gene and genotype/phenotype correlation in subcortical band heterotopia. Eur J Hum Genet 9, 5-12 (2001).
58. Deuel, T. A. et al. Genetic interactions between doublecortin and doublecortin-like kinase in neuronal migration and axon outgrowth. Neuron 49, 41-53 (2006).
59. Koizumi, H., Tanaka, T. & Gleeson, J. G. Doublecortin-like kinase functions with doublecortin to mediate fiber tract decussation and neuronal migration. Neuron 49, 55-66 (2006).
60. Hirotsune, S. et al. Graded reduction of Pafah1b1 (Lis1) activity results in neuronal migration defects and early embryonic lethality. Nat Genet 19, 333-9 (1998).
61. McManus, M. F., Nasrallah, I. M., Pancoast, M. M., Wynshaw-Boris, A. & Golden, J. A. Lis1 is necessary for normal non-radial migration of inhibitory interneurons. Am J Pathol 165, 775-84 (2004).
62. Sanada, K., Gupta, A. & Tsai, L. H. Disabled-1-regulated adhesion of migrating neurons to radial glial fiber contributes to neuronal positioning during early corticogenesis. Neuron 42, 197-211 (2004).
63. Rakic, P. Neuron-glia relationship during granule cell migration in developing cerebellar cortex. A Golgi and electronmicroscopic study in Macacus Rhesus. Journal of Comparative Neurology 141, 283-312 (1971).
64. Gregory, W. A., Edmondson, J. C., Hatten, M. E. & Mason, C. A. Cytology and neuron-glial apposition of migrating cerebellar granule cells in vitro. J Neurosci 8, 1728-38 (1988).
65. Rivas, R. J. & Hatten, M. E. Motility and cytoskeletal organization of migrating cerebellar granule neurons. J Neurosci 15, 981-9 (1995).
66. Gupta, A. et al. Layering defect in p35 deficiency is linked to improper neuronal-glial interaction in radial migration. Nat Neurosci 6, 1284-91 (2003).
67. Tanaka, T. et al. Cdk5 phosphorylation of doublecortin ser297 regulates its effect on neuronal migration. Neuron 41, 215-27 (2004).
68. Ward, M. E., Jiang, H. & Rao, Y. Regulated formation and selection of neuronal processes underlie directional guidance of neuronal migration. Mol Cell Neurosci 30, 378-87 (2005).
69. Liu, G. & Rao, Y. Neuronal migration from the forebrain to the olfactory bulb requires a new attractant persistent in the olfactory bulb. J Neurosci 23, 6651-9. (2003).
70. Mimori-Kiyosue, Y., Shiina, N. & Tsukita, S. The dynamic behavior of the APC-binding protein EB1 on the distal ends of microtubules. Curr Biol 10, 865-8 (2000).
71. Rubinson, D. A. et al. A lentivirus-based system to functionally silence genes in primary mammalian cells, stem cells and transgenic mice by RNA interference. Nat Genet 33, 401-6 (2003).

72. Miyoshi, H., Blomer, U., Takahashi, M., Gage, F. H. & Verma, I. M. Development of a self-inactivating lentivirus vector. J Virol 72, 8150-7 (1998).

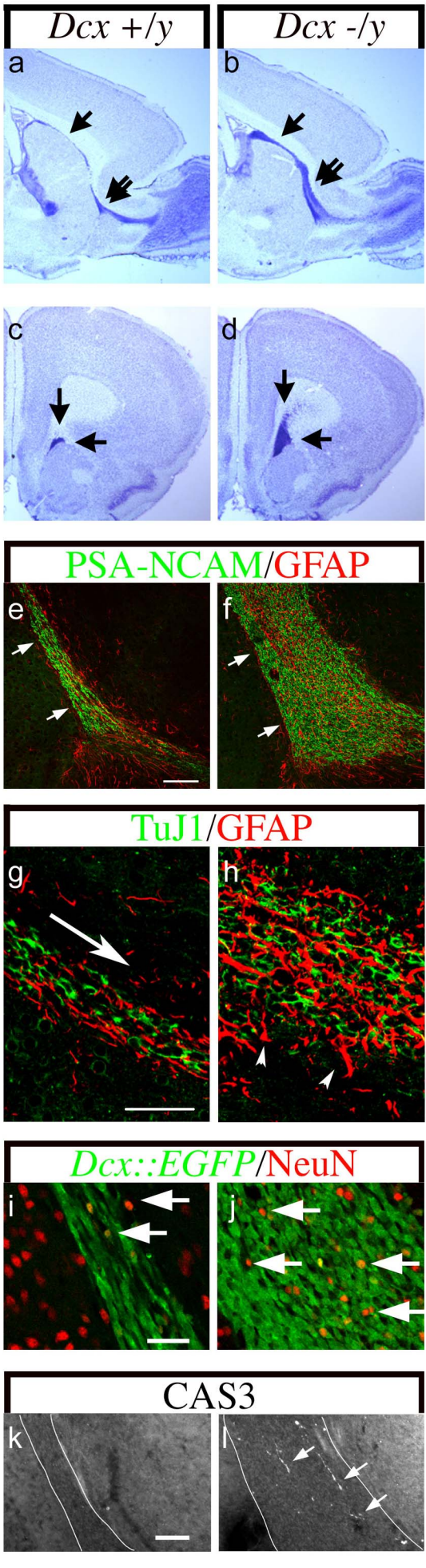
Dcx +/y
Dcx -/y
a
b
c
d
PSA-NCAM/GFAP
e
f
TuJ1/GFAP
g
h
Dcx::EGFP/NeuN
i
j
CAS3
k
l

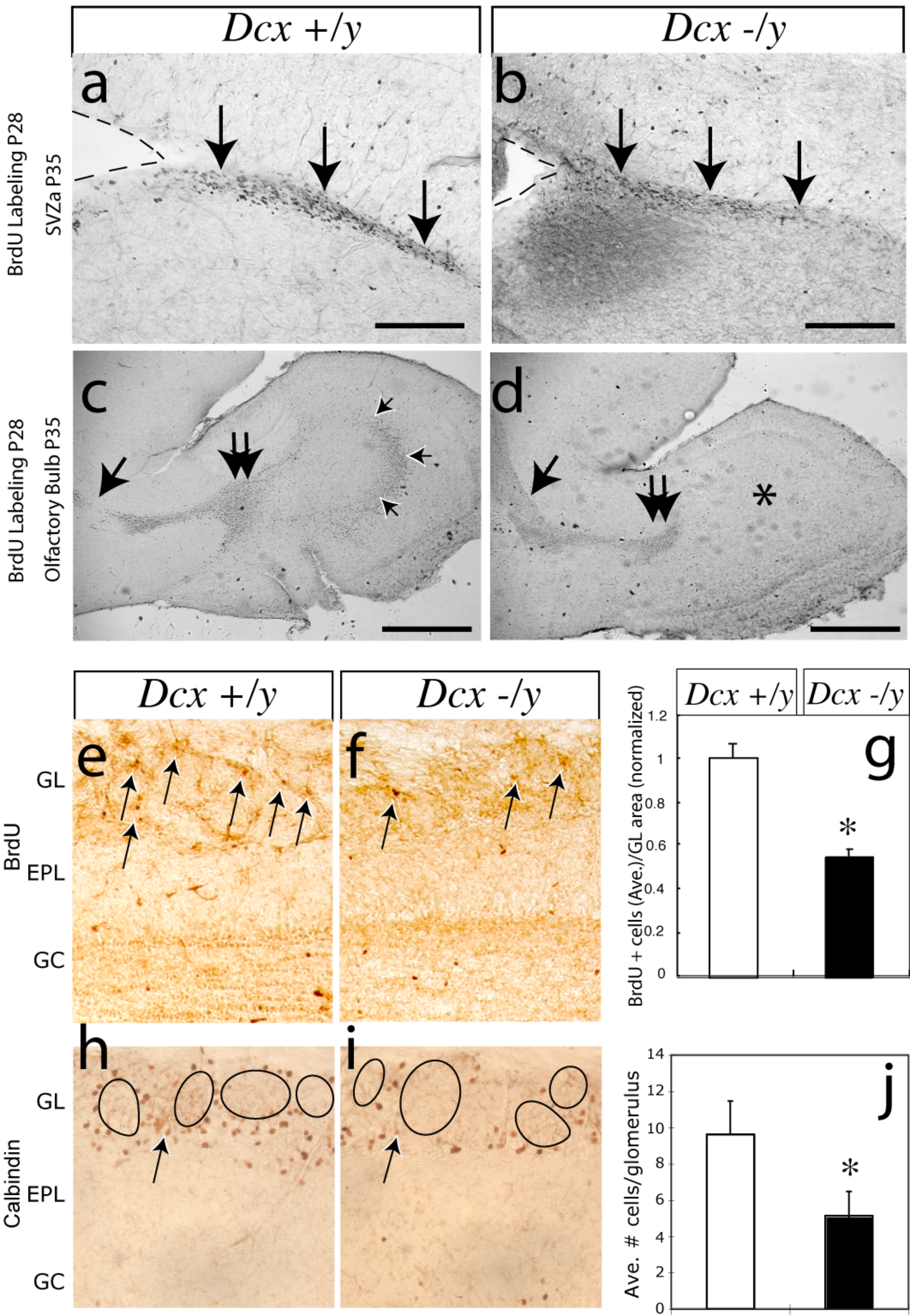
Dcx +/y
Dcx -/y
a
b
BrdU Labeling P28
SVZa P35
c
d
BrdU Labeling P28
Olfactory Bulb P35
Dcx +/y
Dcx -/y
e
f
GL
EPL
GC
BrdU
g
BrdU + cells (Ave.)/GL area (normalized)
1.2
1
0.8
0.6
0.4
0.2
0
h
i
GL
EPL
GC
Calbindin
j
Ave. # cells/glomerulus
14
12
10
8
6
4
2
0

a

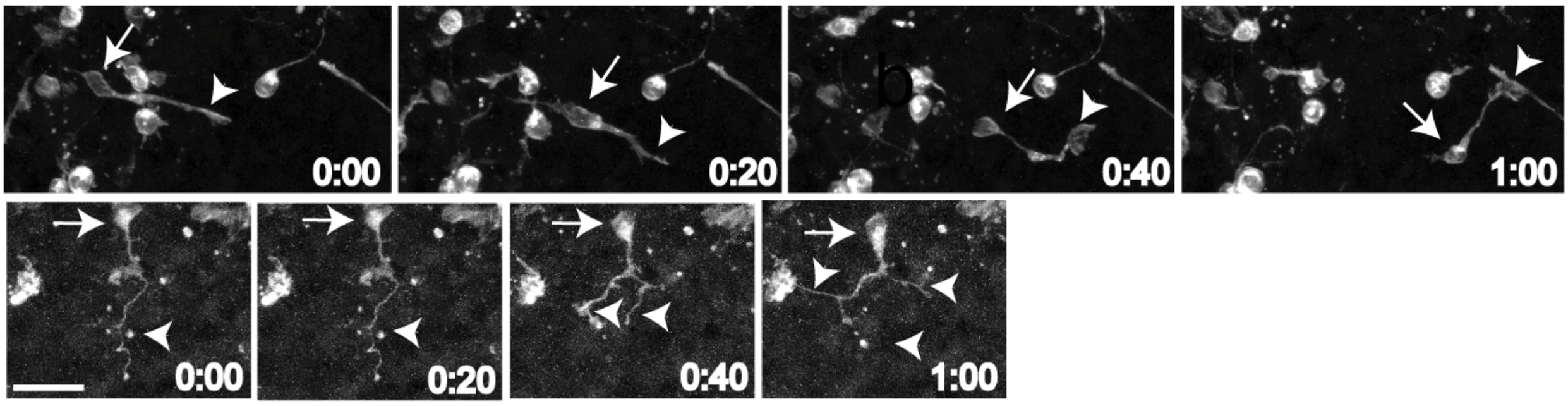

b

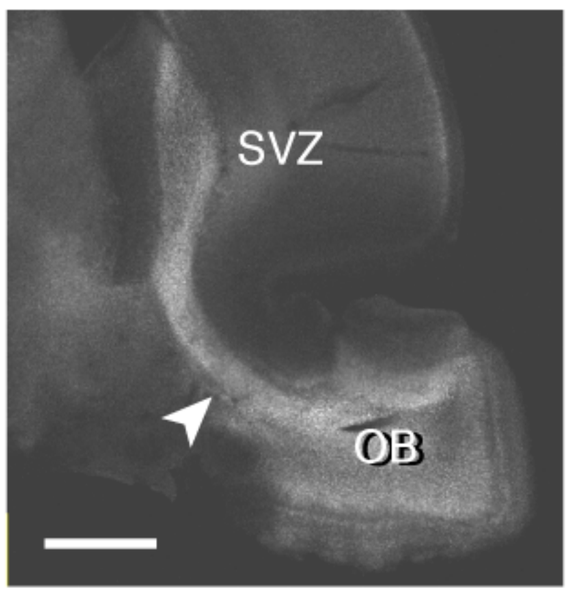

Dcx::EGFP P5

c

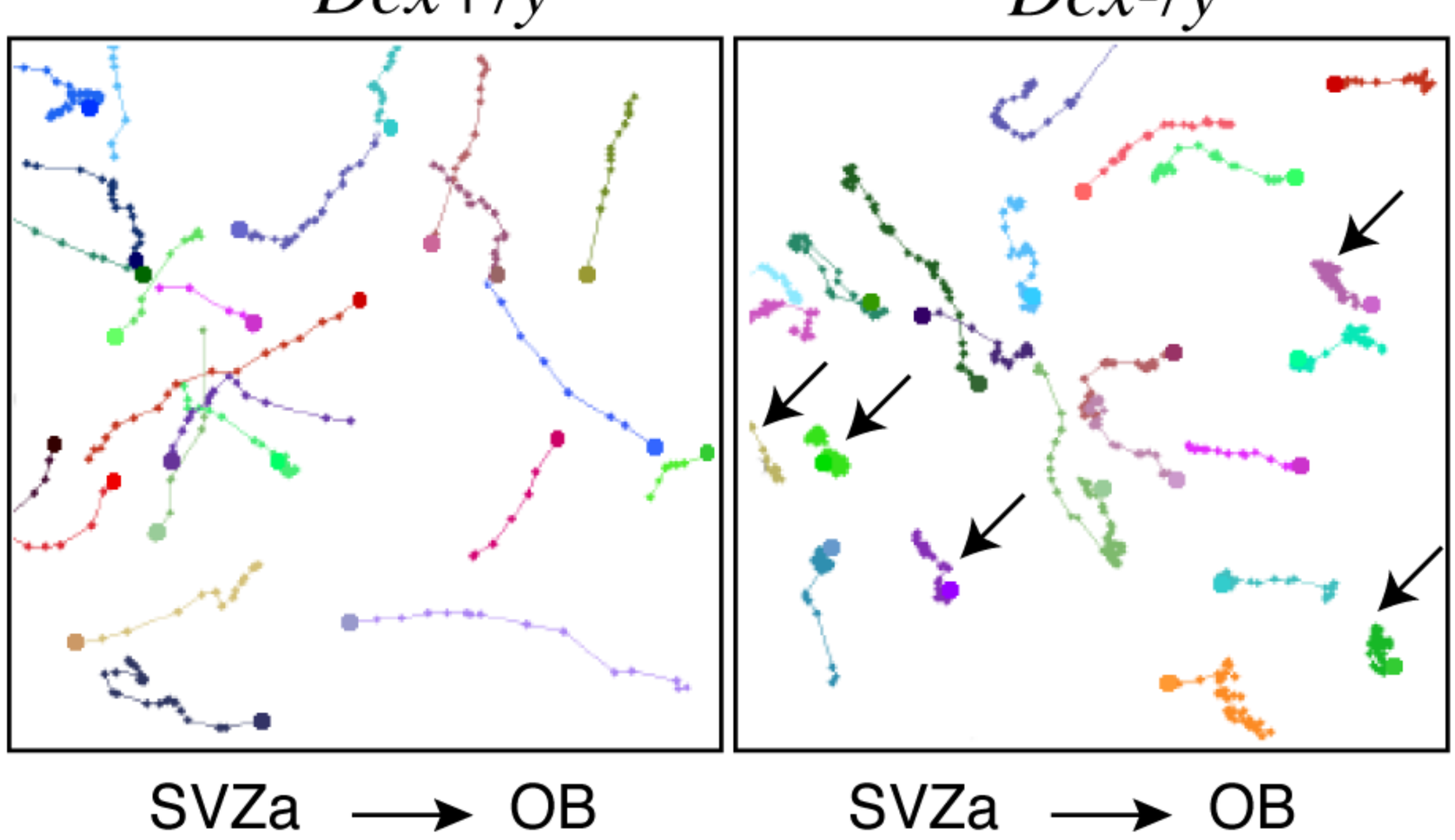

d

e

f

Direction	*Dcx +/y*	*Dcx -/y*
SVZ->OB	47.2	43.2
OB->SVZ	47.2	47.7
SVZ<->OB	6.3	6.9

g

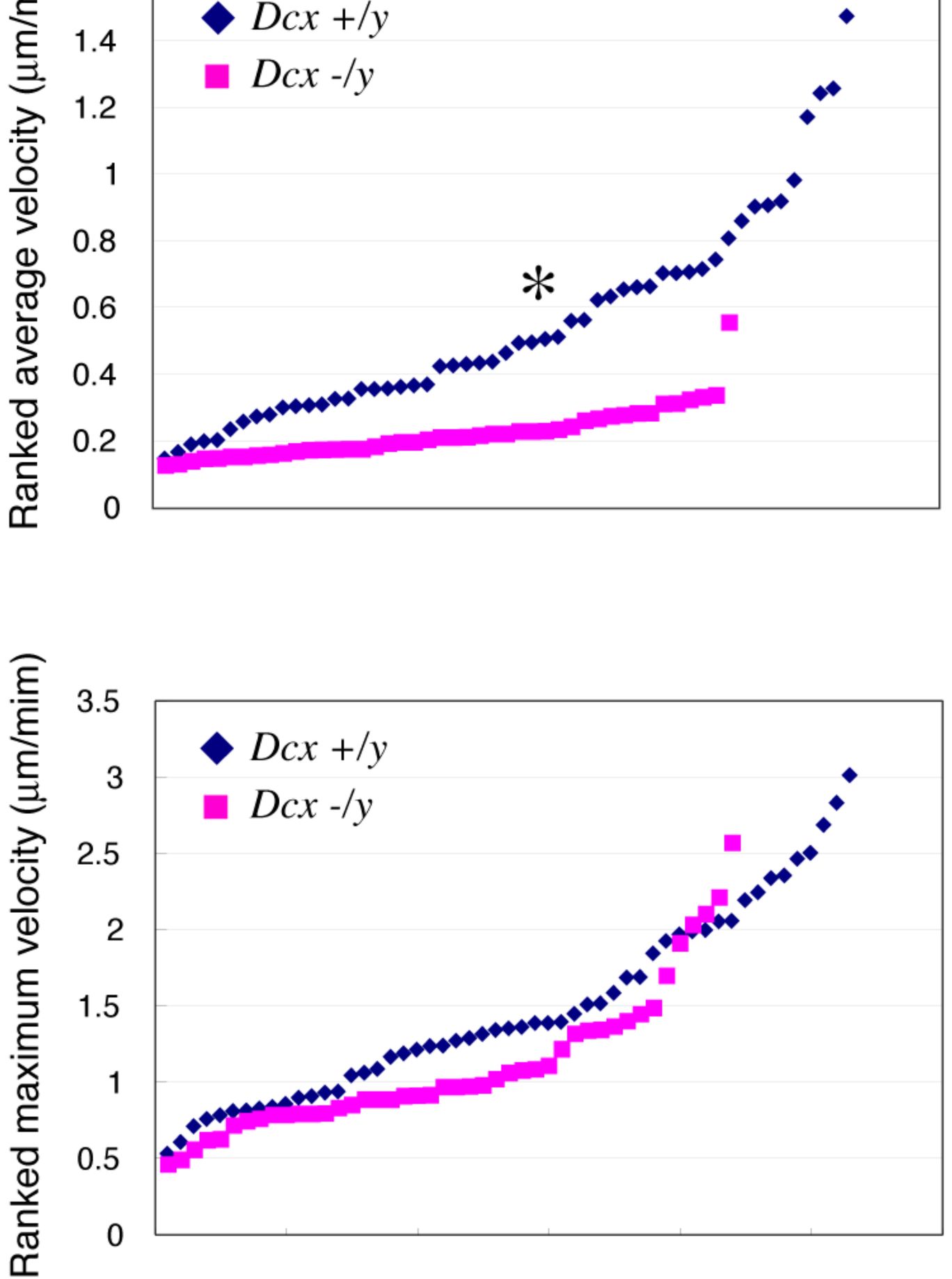

a

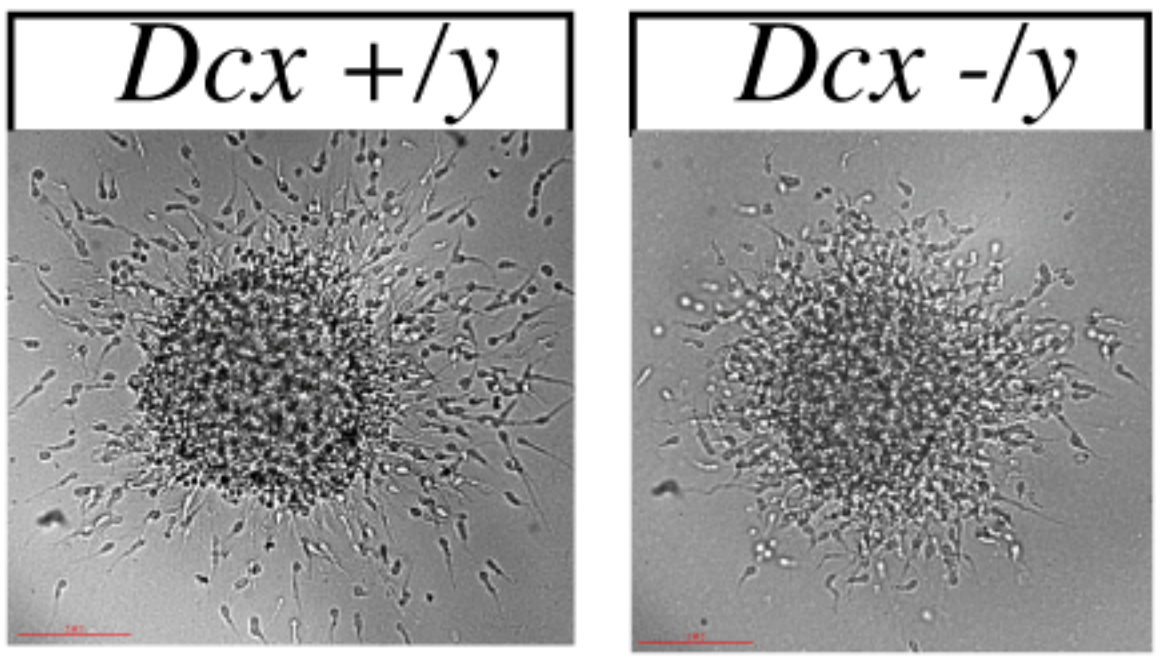
Dcx +/y
Dcx -/y
Phase

b

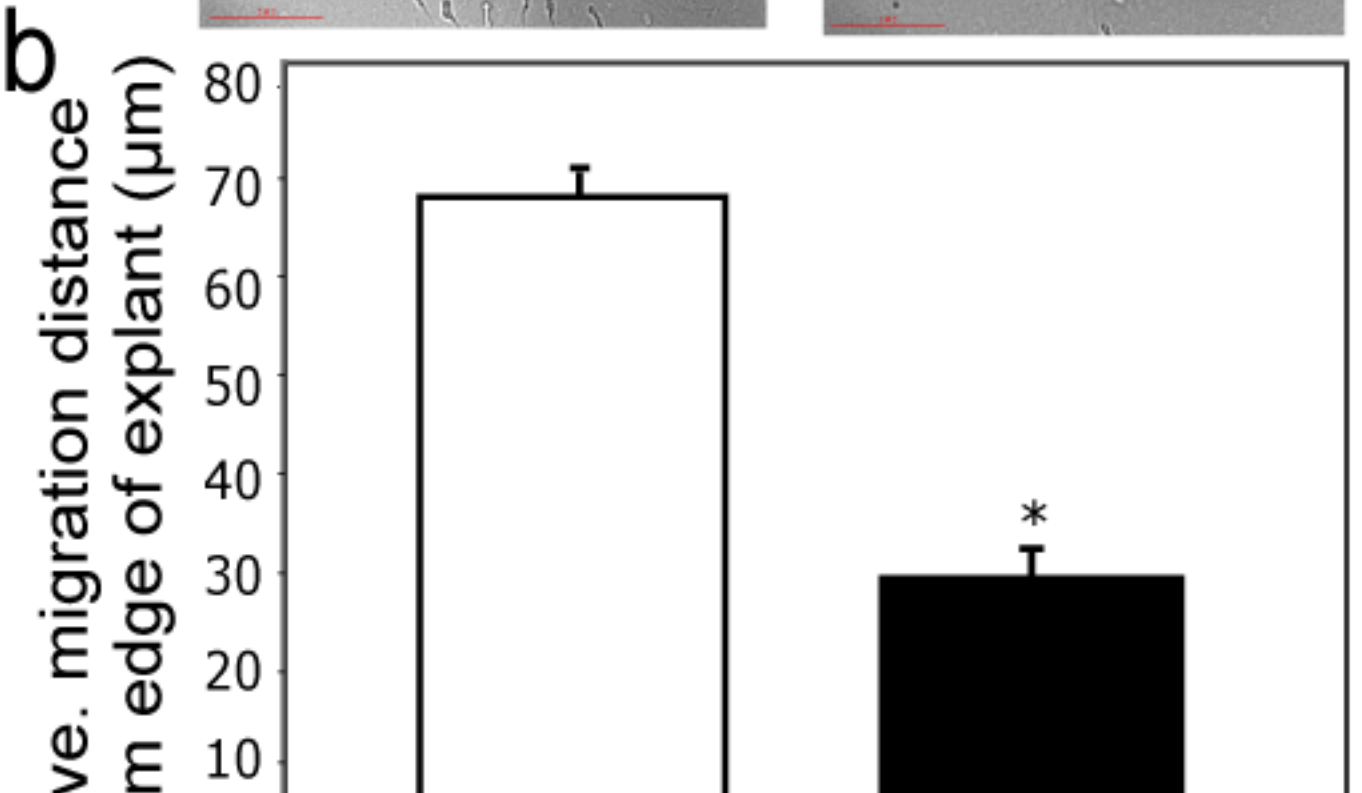
Ave. migration distance from edge of explant (μm)
80
70
60
50
40
30
20
10
0
*

c

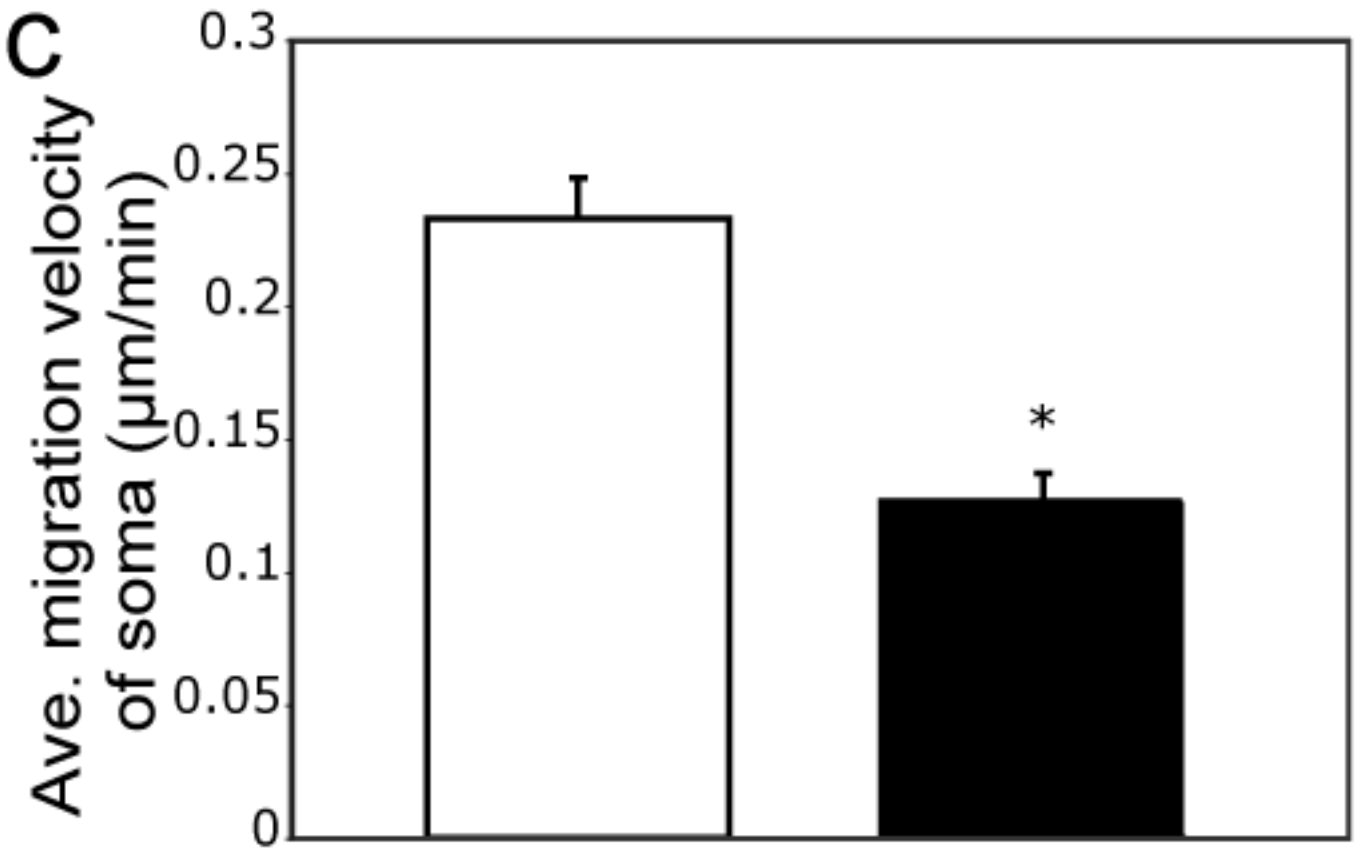
Ave. migration velocity of soma (μm/min)
0.3
0.25
0.2
0.15
0.1
0.05
0
*

d

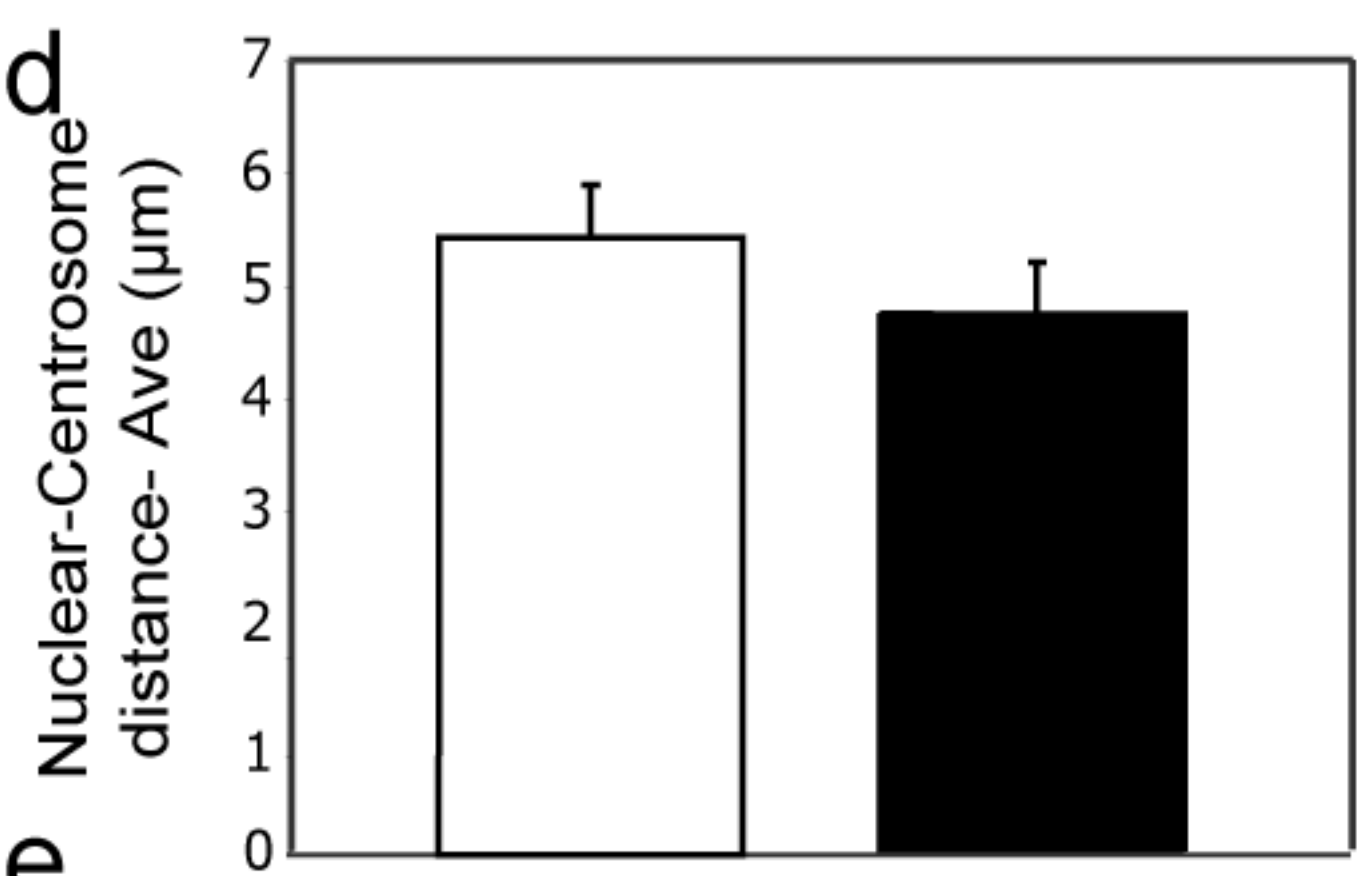
Nuclear-Centrosome distance- Ave (μm)
7
6
5
4
3
2
1
0

e

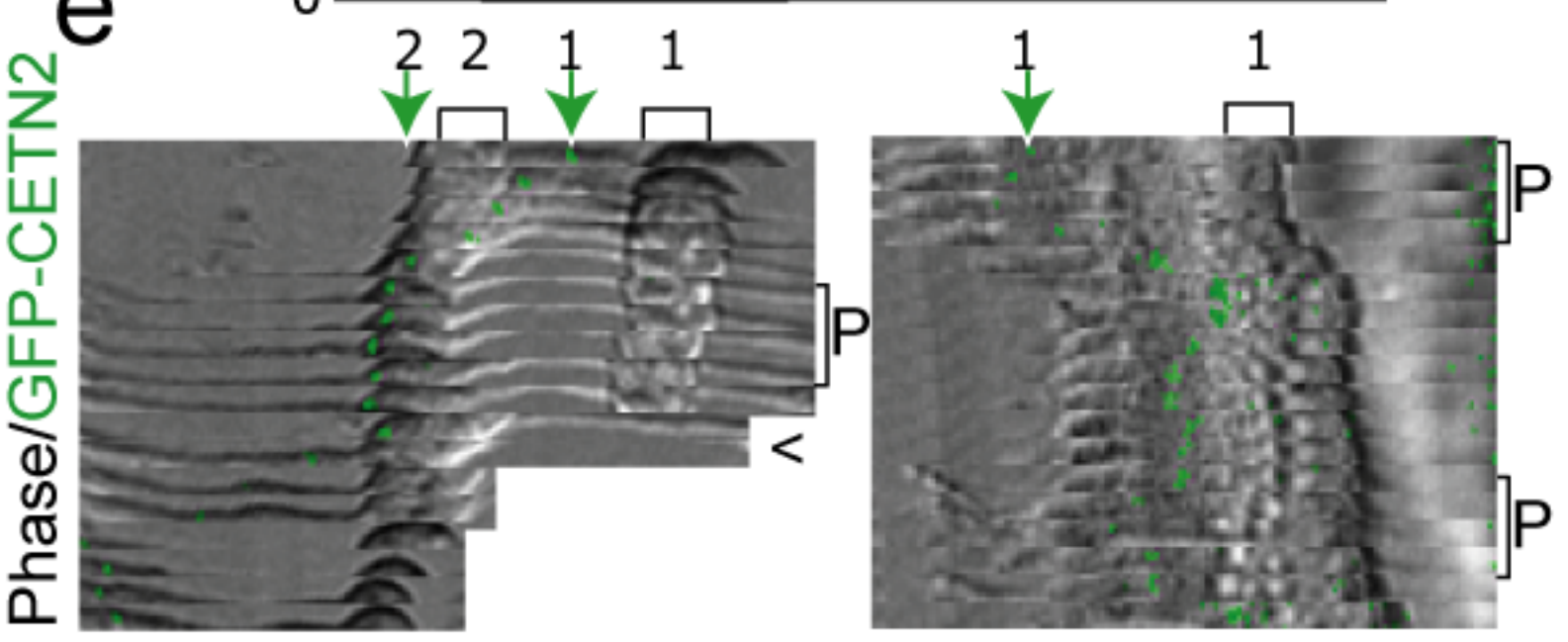
Phase/GFP-CETN2
2
2
1
1
1
1
P
P
P

f

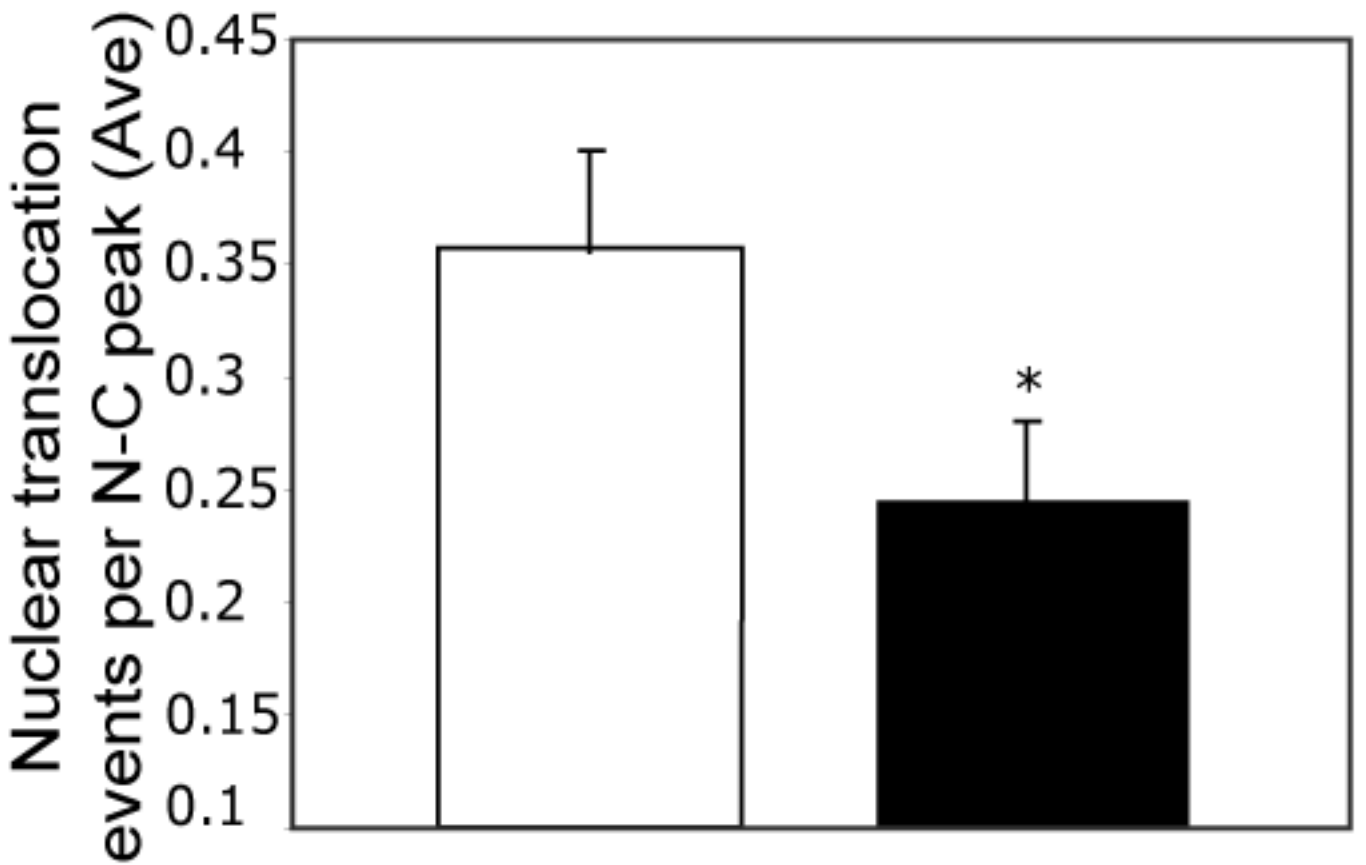
Nuclear translocation events per N-C peak (Ave)
0.45
0.4
0.35
0.3
0.25
0.2
0.15
0.1
*

a

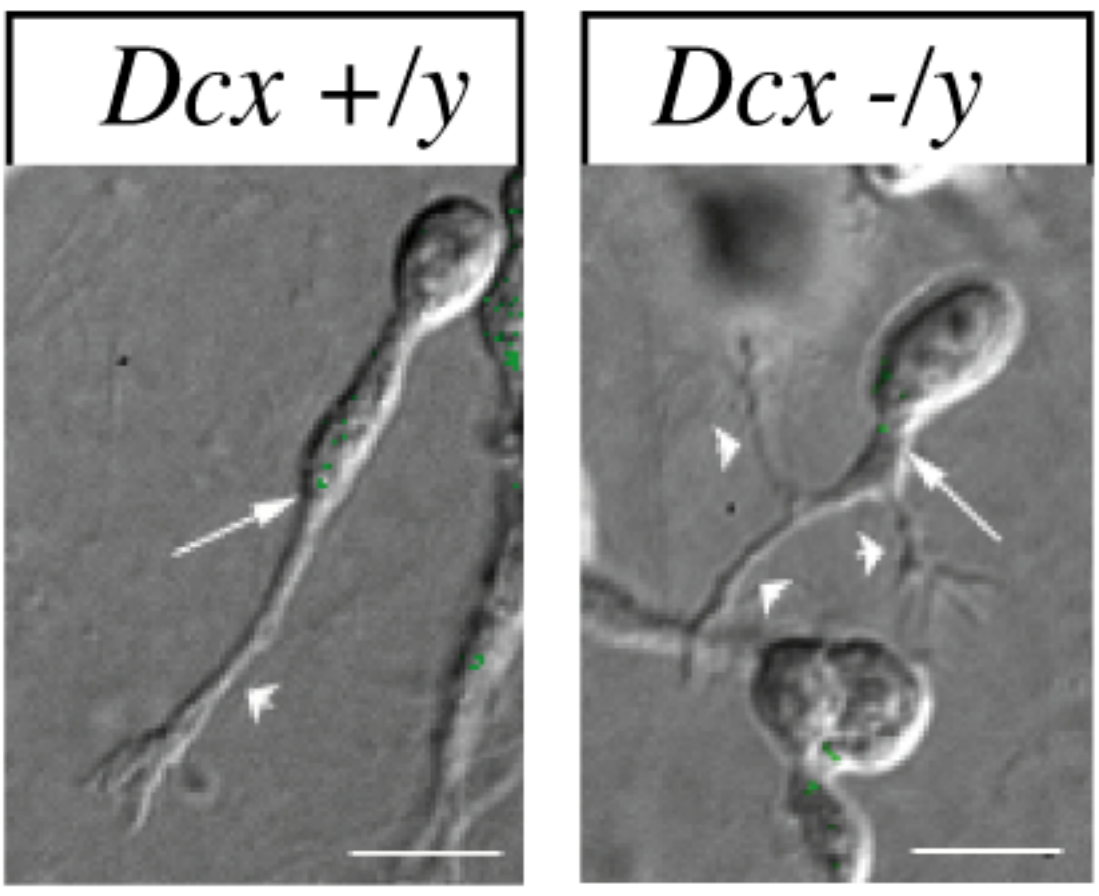
Dcx +/y
Dcx -/y

b

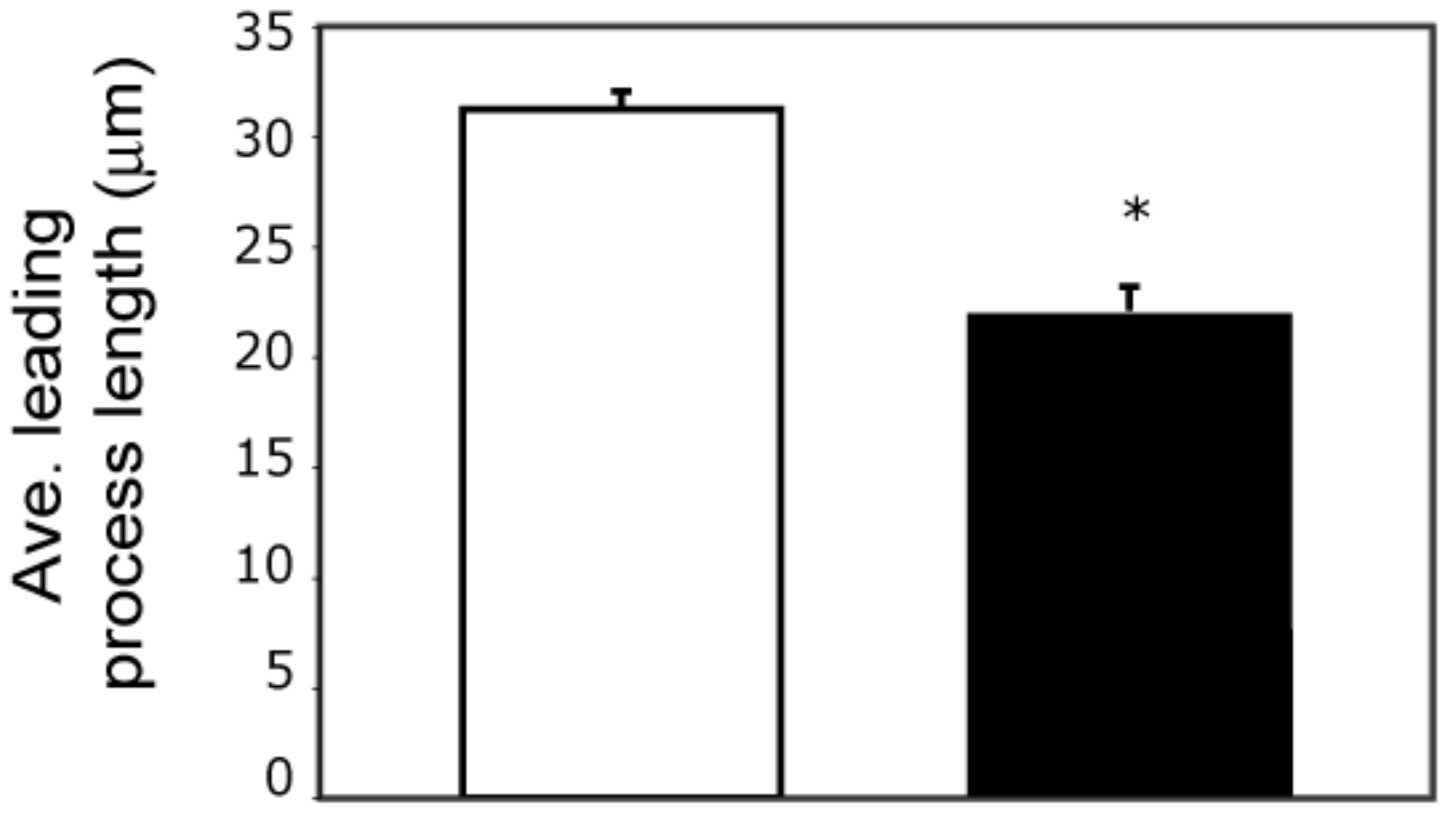
Ave. leading process length (μm)
35
30
25
20
15
10
5
0
*

c

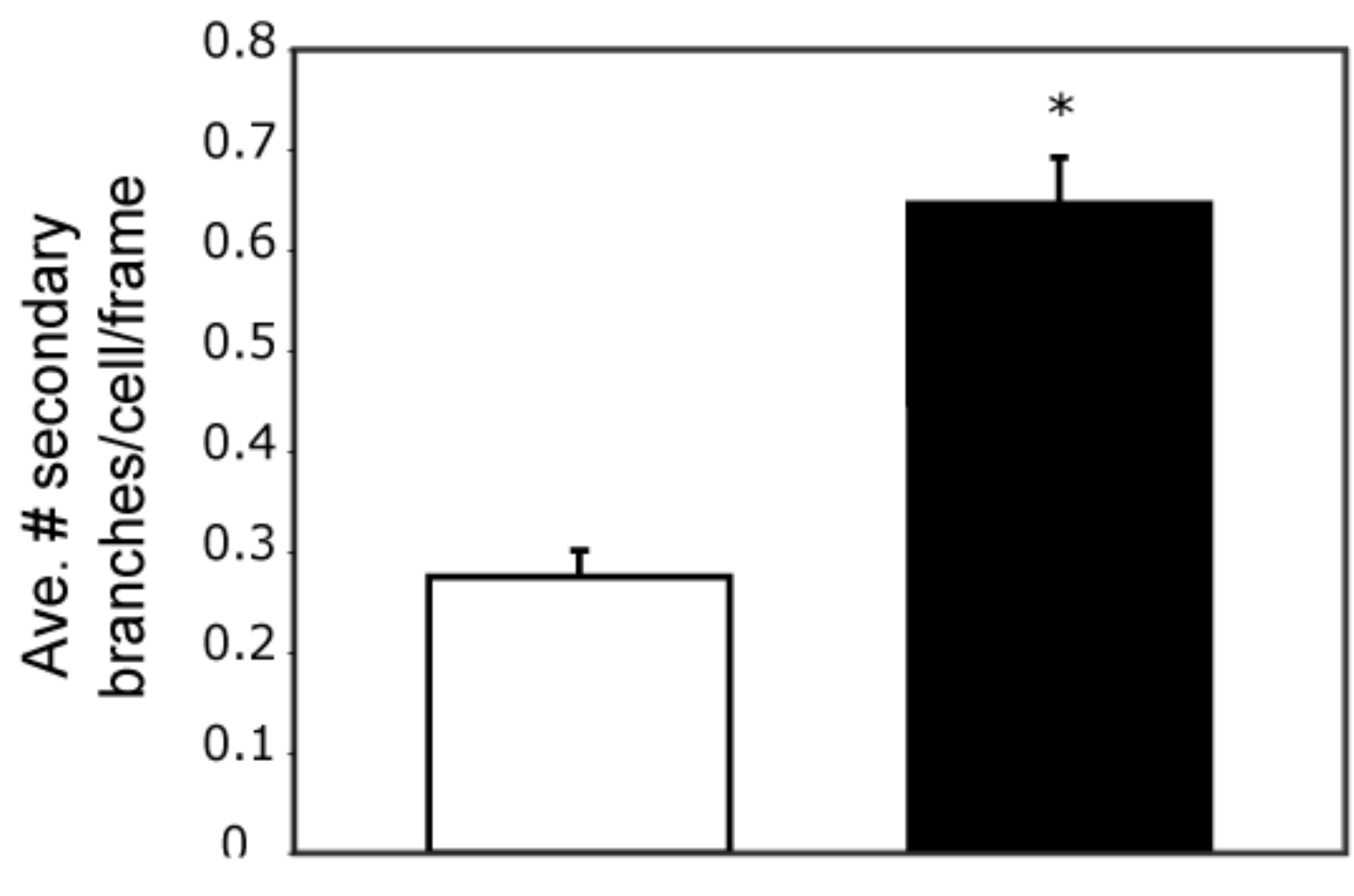
Ave. # secondary branches/cell/frame
0.8
0.7
0.6
0.5
0.4
0.3
0.2
0.1
0
*

d

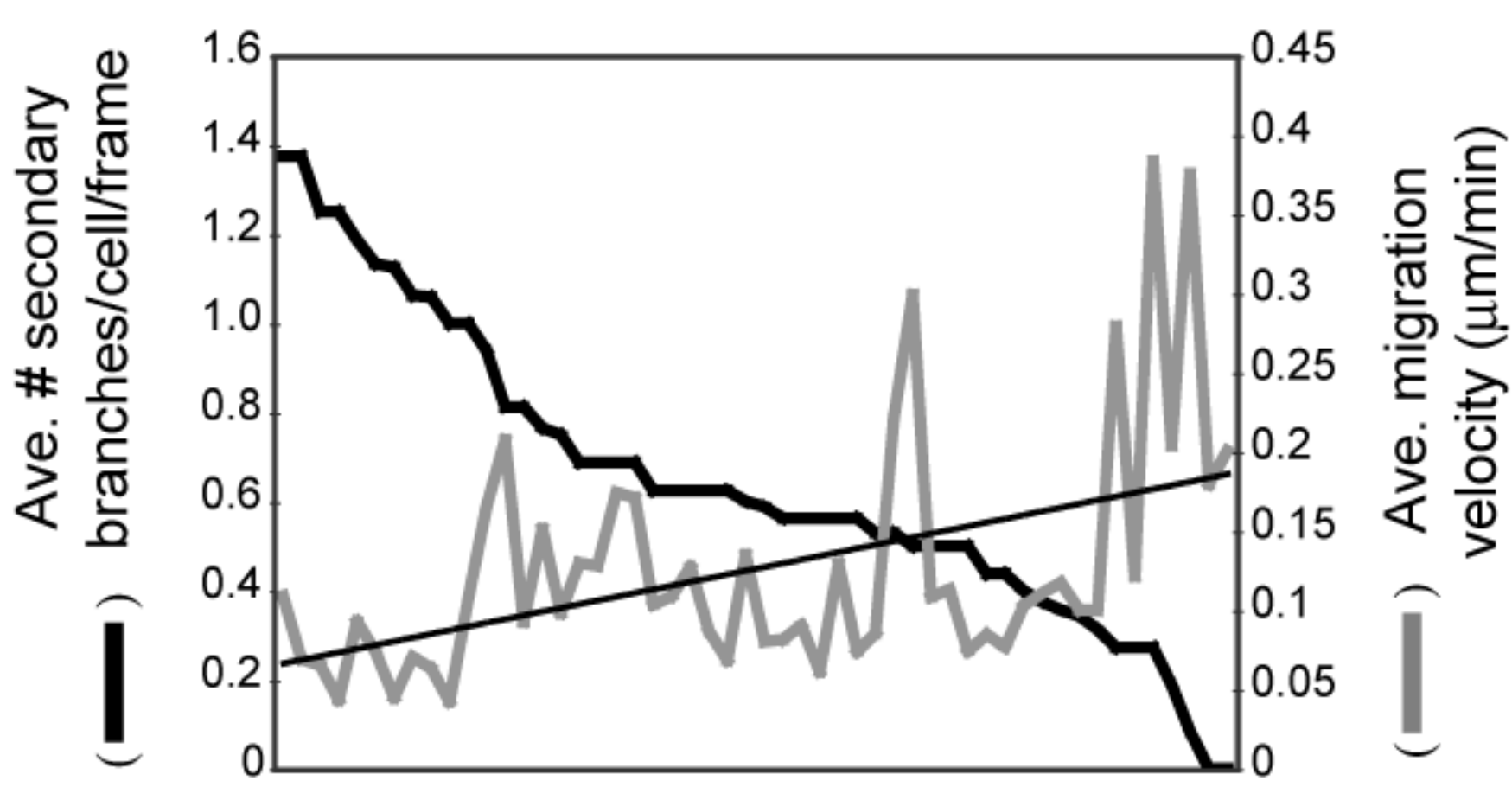
Ave. # secondary branches/cell/frame
Ave. migration velocity (μm/min)
1.6
1.4
1.2
1.0
0.8
0.6
0.4
0.2
0
0.45
0.4
0.35
0.3
0.25
0.2
0.15
0.1
0.05
0

e

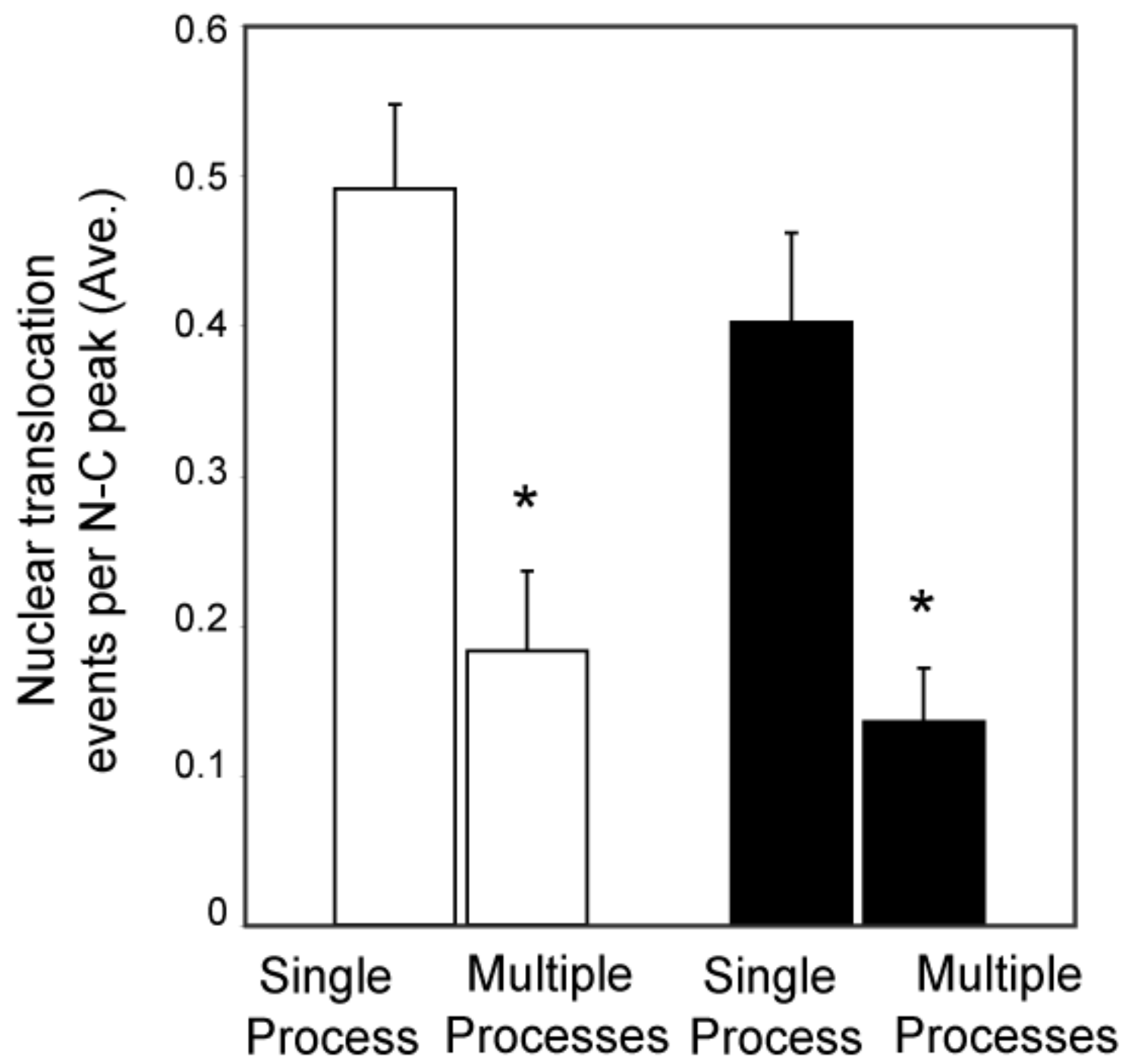
Nuclear translocation events per N-C peak (Ave.)
0.6
0.5
0.4
0.3
0.2
0.1
0
*
*
Single Process
Multiple Processes
Single Process
Multiple Processes